IDA

INSTITUTE FOR DEFENSE ANALYSES

General Approach to Template-Based Target Recognition

J. Kent Haspert
James F. Heagy
Roger J. Sullivan

March 2005

IDA Paper NS P-3981
Log: H 05-000079

This work was conducted under contract DASW01 04 C 0003, IDA Central Research Project C2081. The publication of this IDA document does not indicate endorsement by the Department of Defense, nor should the contents be construed as reflecting the official position of that Agency.

INSTITUTE FOR DEFENSE ANALYSES

IDA Paper NS P-3981

General Approach to Template-Based Target Recognition

J. Kent Haspert
James F. Heagy
Roger J. Sullivan

PREFACE

This paper was prepared under an IDA Central Research Project titled "Application Theory of Target Recognition."

The authors wish to thank two of our colleagues, Amnon Dalcher and Michael Tuley, who have reviewed this paper and made some valuable suggestions. In particular, Dr. Dalcher suggested that the strange behavior being observed at low SNRs for the noncoherent case could be due to the need to employ a square-law detector at low signal-to-noise levels. This questioning led to the revised formulation presented in Section V.C. Mr. Tuley asked whether our use of the Brennan and Reed criterion, while maximizing SNR, would also lead to maximum discrimination between two targets; Dr. Dalcher described the criterion's relationship to the discriminability criteria test. Mr. Tuley also provided support to our concern about the feasibility of being able to make accurate phase measurements at low SNR values.

CONTENTS

I. Introduction I-1

II. Confusion Matrices II-1

III. Target Representations III-1

IV. Mathematical Procedures for Target Recognition IV-1

V. Example Cases V-1
- A. Independent Targets—Coherent Processing V-1
- B. Correlated Targets—Coherent Processing V-4
- C. Correlated Targets—Noncoherent Processing V-7

VI Practical Considerations VI-1
- A. Uncertainties Associated with Coherent Processing VI-1
- B. Target Scintillation Effects VI-2
- C. Effect of Total Target Return on Noise Values VI-2
- D. Evaluation of Target Classes and Target Fluctuations VI-3
- E. Evaluation of Non-isotropic Noise VI-5
- F. Discrimination Among Targets Within a Class VI-6
- G. Dealing with a Mix of Highly Correlated and Nearly Uncorrelated Targets VI-7
- H. Effect of Dimensionality of Target Template Vectors VI-8

VII. Conclusions VII-1

Appendix—Proofs A-1

FIGURES

1. Basis for Cross-Range Measurement 1-2
2. Representative Confusion Matrix II-2
3. Simple Probability Example II-3
4. Simple Target Representation III-2
5. Depiction of Expected Values of Test Statistics in the Complex Plane and Possible Comparisons Between Them IV-2
6. Diagonal Matrix Element as a Function of SNR for Independent Targets V-3
7. Diagonal Matrix Element as a Function of SNR for Two Correlated Targets V-7
8. Three Hypothetical Templates Represented by Matrices in (40) V-9
9. P_{11} vs. SNR for Pairwise Comparison of Targets 1 and 2 in Figure 8 .... V-10
10. P_{11} and P_{33} vs. SNR Pairwise Comparison of Targets 1 and 3 in Figure 8 Demonstrates a Flaw in our Direct Use of a Linear Process V-11
11. Corrected Results of P_{11} and P_{33} vs. SNR with Revised Templates for Targets 1 and 3 .... V-13
12. Longitudinal Phase Difference Geometry VI-1
13. Scintillation Geometry VI-2
14. Variation in Magnitude of Return as Angle Changes VI-3
15. Formation of Target Class Templates VI-4
16. “Noise” for Target Class VI-5
17. Non-isotropic Noise Case VI-6
18. Effect of Removing the Target Class Vector VI-7
19. Mix of Highly Correlated and Uncorrelated Targets VI-8
20. Effect of Dimensionality on Dot Products (Constant Correlation) VI-11
21. Effect of Variable Correlation on Vector Dot Products VI-11

TABLE

1. SNR-Dependent Noncoherent Target Templates V-12

I. INTRODUCTION

Target identification remains a challenging problem for air combat, due often to the lack of an adequate number of ways to determine identities of all targets. High range resolution (HRR) radar offers a potential additional source of target identification information [1]. HRR employs a high-bandwidth radar signal to find the locations and relative intensities of the radar scatterers along the longitudinal axis of a target. The range resolution, Δ_R, is given by $\Delta_R \sim c / 2B$, where c is the speed of light and B is the radar's bandwidth. For example, a radar bandwidth of 150 MHz provides 1 m range resolution. A radar with this bandwidth could collect 30 separate radar cross-section measurements along the length of a 30 m long aircraft. One form of HRR involves merely determining the distance between the first and last return from a target to discern its length and thereby yield a simple target classification (e.g., fighter, bomber, cruise missile). A more sophisticated approach involves measuring each of the returns along the target's length and comparing the locations and relative intensities of the observed scatterers to prestored target templates. The second approach typically produces more detailed target classification (e.g., F-15, MiG-29).

Range-Doppler-imaging (RDI) radar offers an alternative way to use radar measurements to classify targets. Synthetic aperture radar (SAR) involves an airborne radar viewing a ground target from various angles (as the radar flies by or around the target) to create a two-dimensional image of the target. RDI, on the other hand, uses a relatively stationary radar to observe an airborne target from different angles as the target maneuvers or flies by the radar.[1] As with SAR, RDI forms a two-dimensional image of the target by employing HRR techniques to detect scatterers in the radial direction from the radar and observing relative Doppler shifts to determine the cross-range position of the scatterers (see Figure 1, which illustrates relative velocity differences as a function of distance from the centroid of the target and rate of apparent target rotation).

---

1 The stationary radar could correspond to a fixed ground radar site. Alternatively, the "stationary" radar could be on a moving aircraft, but all the target measurements would be made with respect to a moving coordinate system that moves with the radar. Also, if the target is maneuvering in both a horizontal and vertical plane, then a 3-D image might be formed [2], but we will not consider this 3-D case in this paper.

Although a two-dimensional image would surely be more recognizable by a human, we wish to find an analytical basis for quantifying the inherent differences between target identification based on one-dimensional and two-dimensional target signatures. Our approach starts by representing a set of expected targets (either one-dimensional or two-dimensional) as templates, typically multidimensional complex vectors.

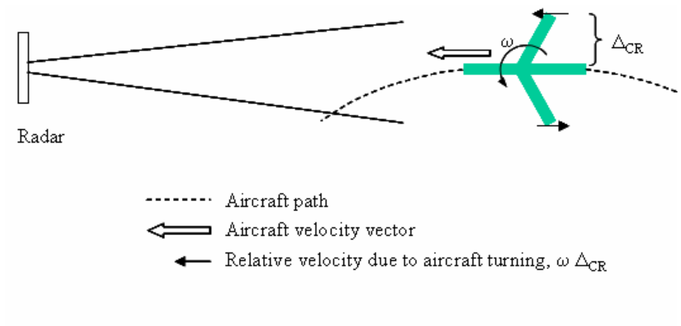

Figure 1. Basis for Cross-Range Measurement

Applying a matched-filter computational process (Sections III and IV), the vector templates are compared with a target return signal (corrupted by noise) to produce a set of scalar test statistics. The test statistics are compared and their associated probabilities of observation are estimated. These probabilities represent the probabilities of correct and incorrect target classification. The probabilities are typically presented in the form of confusion matrices (Chapter II). The details of these calculations depend on the statistics chosen and on the assumptions regarding the characteristics of the interference (noise, jamming, clutter) associated with the radar measurements. These noise characteristics govern the degree to which correct and incorrect classifications can occur. Some simple example calculations are presented in Chapter V. The methodology reported herein should provide insight into the underlying issues associated with target identification. Whereas these analyses are purely theoretical, in Chapter VI we discuss ways to extend the analyses to include real-world issues associated with target identification.

II. CONFUSION MATRICES

Confusion matrices provide a convenient format for representing the degree to which an identification process can correctly or incorrectly classify targets. If confusion matrices exist for multiple sensors, then the confusion matrices can be combined relatively easily to evaluate the result of a fused-identification (ID) decision [3]. We will define the rows of the matrix to correspond to true target types; the columns then represent the possible outputs of the identification sensor (sometimes the definitions for the rows and columns are interchanged). In general, the column headers need not correspond to the row labels. For example, the rows could represent F-15, F-16, MiG-29, B-52, and Silkworm. A sensor that determines only the relative length of such targets might only provide the following outputs: long, medium, and short, which would then serve as the column headers for the sensor's confusion matrix. However, for the purposes of this paper, we wish to consider the special case of confusion matrices that have column headers that correspond to the row labels, for reasons that will become clear later on. Each row of the confusion matrix represents the conditional probability of each possible sensor output if the target were truly of the type defined by the row label. An ideal confusion matrix of this form would equal the identity matrix with probabilities of one on the diagonal and zeros elsewhere. A highly desirable (and potentially more feasible) confusion matrix would have its highest values along the diagonal but would inevitably have some probabilities in the off-diagonal elements. In any case, the row entries of a probability matrix must add to one, since the columns represent the set of all possible sensor outputs for the given true target. In the interest of improving the ratio of the probabilities of correct to incorrect reports from an identification sensor, we will also consider the case of an optional extra column that corresponds to an unknown or no declaration, as shown in Figure 2. In Figure 2, $P(t_2|t_1)$ represents the probability of declaring target 2 when target 1 is actually being observed.

This paper addresses a method to derive the conditional probability entries for these confusion matrices for both one-dimensional and two-dimensional target ID sensors (and even three-dimensional sensors if they should exist).

		Sensor Output			
		Target 1	Target 2	Target 3	No Declare
True Target Type	Target 1	$P(\mathrm{t}_1 \mid \mathrm{t}_1)$	$P(\mathrm{t}_2 \mid \mathrm{t}_1)$	$P(\mathrm{t}_3 \mid \mathrm{t}_1)$	$P(\mathrm{ND} \mid \mathrm{t}_1)$
	Target 2	$P(\mathrm{t}_1 \mid \mathrm{t}_2)$	$P(\mathrm{t}_2 \mid \mathrm{t}_2)$	$P(\mathrm{t}_3 \mid \mathrm{t}_2)$	$P(\mathrm{ND} \mid \mathrm{t}_2)$
	Target 3	$P(\mathrm{t}_1 \mid \mathrm{t}_3)$	$P(\mathrm{t}_2 \mid \mathrm{t}_3)$	$P(\mathrm{t}_3 \mid \mathrm{t}_3)$	$P(\mathrm{ND} \mid \mathrm{t}_3)$

Figure 2. Representative Confusion Matrix

Before discussing procedures for calculating the entries in a confusion matrix, consider the simple problem[2] posed below:

- Let $\boldsymbol{X}$ be a random variable uniformly distributed between 0 and A.
- Let $\boldsymbol{Y}$ be an independent random variable uniformly distributed between 0 and B.
- What is the probability that $\boldsymbol{X} > \boldsymbol{Y}$?

From basic probability theory, the probability density of $\boldsymbol{X} = x$ is given by $f_x(x) = 1/A$. Similarly, $f_y(y) = 1/B$. Because $\boldsymbol{X}$ and $\boldsymbol{Y}$ are independent, their joint probability density factors, that is, $f(x,y) = f_x(x) \cdot f_y(y) = 1/AB$. If $A \geq B$, then the probability of $\boldsymbol{X} > \boldsymbol{Y}$ is given by

$$\begin{aligned} P(\boldsymbol{X} > \boldsymbol{Y}) &= \int_0^B dy \int_y^A f(x,y)dx = \frac{1}{AB}\int_0^B (A-y)dy \\ &= 1 - \frac{B}{2A} \end{aligned} \quad . \tag{1}$$

The second integral corresponds to summing the horizontal differential strips shown in Figure 3. If vertical strips were summed instead, then the following integral would apply:

$$P(\boldsymbol{X} > \boldsymbol{Y}) = \int_{\min(X)}^{\max(X)} \left[\int_{\min(Y)}^{\min(x,\max(Y))} f(x,y)dy \right] dx \; . \tag{2}$$

[2] A reader well versed in probability theory could skip to Chapater III, but the following equations will be applied in subsequent sections of the paper.

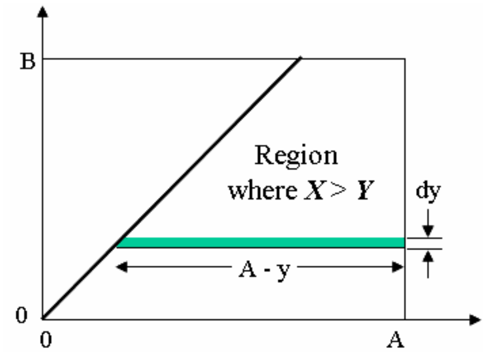

Figure 3. Simple Probability Example

Notice that as now formulated, the probability of $\boldsymbol{X} > \boldsymbol{Y}$ would come from the same general equation (2) regardless of the domain of the random variables $\boldsymbol{x}$ and $\boldsymbol{y}$. Moreover, the joint probability function, $f(x, y)$, need not be uniform. That is, if $f(x, y) = f_{T1}(x, y)$ represents the joint probability of a sensor providing either an X or a Y indication when the true target is type t_1, then (2) would generate the conditional probability $P(X|t_1)$—the probability that an X indication would be provided when the true target type is t_1. If the identification sensor *only* has outputs X or Y, then $P(Y|t_1) = 1 - P(X|t_1)$. If the joint probability function is defined over all real numbers, then $\min(X) = -\infty$, $\min(Y) = -\infty$, $\max(X) = \infty$, and $\min(x, \max(Y)) = x$.

If the identification sensor has three possible outputs (X, Y, and Z) with probabilities defined over all real numbers, then a similar process could be used to find the probability that output X occurs (i.e., the probability that the random variable x has the largest value) when the true target type is t_i, as follows:

$$P(X|t_i) = P(x > y \text{ and } x > z) = \int_{-\infty}^{\infty} dx \int_{-\infty}^{x} dy \int_{-\infty}^{x} f_{Ti}(x, y, z) dz \ . \tag{3}$$

Equation (3) extends to any number of output states in an obvious way. If we further assume that the random variables $\boldsymbol{x}$, $\boldsymbol{y}$, and $\boldsymbol{z}$ are independent, that is, $f_{Ti}(x, y, z) = f_{Xi}(x)\, f_{Yi}(y)\, f_{Zi}(z)$, and can each range from $-\infty$ to $+\infty$, then:

$$\begin{aligned} P(X|t_i) &= (x > y \text{ and } x > z) \\ &= \int_{-\infty}^{\infty} f_{Xi}(x) dx \left[\int_{-\infty}^{x} f_{Yi}(y) dy \right] \cdot \left[\int_{-\infty}^{x} f_{Zi}(z) dz \right] \\ &= \int_{-\infty}^{\infty} f_{Xi}(x) F_{Yi}(x) F_{Zi}(x) dx \end{aligned} \tag{4}$$

where F_{Yi} and F_{Zi} are the cumulative distributions corresponding to f_{Yi} and f_{Zi}, respectively.

If independence among the random variables associated with each decision is assumed for n possible sensor outputs, labeled X_1 through X_n, then for output X_k:

$$P(X_k \mid T_i) = \int_{-\infty}^{\infty} f_{X_k}(x_k)dx_k \prod_{j \neq k} \int_{-\infty}^{x_k} f_{X_j}(w)dw$$

$$= \int_{-\infty}^{\infty} f_{X_k}(x_k)dx_k \frac{\prod_{j=1}^{n} F_{X_j}(x_k)}{F_{X_k}(x_k)} \tag{5}$$

where the density and cumulative functions correspond to a true target type of t_i.

Equations (3)–(5) all address the case where a sensor decision must be made. There are several ways to include the possibility of "no declaration." For example, one can require the "winning" signal X_k not only to be the largest, but to also exceed a threshold value α,

$$X_k \geq X_j \textit{ and } X_k \geq \alpha \text{ for all } k \neq j. \tag{6}$$

Signals that fail to satisfy this requirement yield a no-declaration designation. A natural choice for the threshold α is to require signals less than or equal to α to capture a prescribed fraction, $p(\alpha)$, of the probability density function (PDF) of the *true* target,

$$p(\alpha) = F_{X_k}(\alpha) = \int_{-\infty}^{\alpha} f_{X_k}(x)dx\,. \tag{7}$$

Users requiring high confidence in making correct target assignments might set p to a high value (say $p = 0.5$); users wishing to force decisions, but not requiring high-confidence decisions, would conversely set p to a low value. The threshold-conditioned confusion matrix entries are found by replacing the lower limits on the integrals in (3), (4), and (5) by the threshold value α. In the event that the X_k variables are independent, it can be shown (see appendix, Section A-1) that the no-declaration probability is given by the simple, and generally obvious, expression

$$P(ND \mid T_i) = \prod_{j=1}^{n} F_{X_j}(\alpha)\,. \tag{8}$$

Alternatively, one can require the winning signal to exceed all other signals by a designated amount ε,

$$X_k \geq X_j + \varepsilon, \text{ for all } k \neq j. \tag{9}$$

For example, one could choose ε to be a measure of the intrinsic noise in the signal x (e.g., ε equals one standard deviation), thus increasing the confidence that the winner is not a statistical outlier. When imposing condition (9), the confusion matrix entries are found by setting the upper limits of the interior integrals (all integrals except for the final integral over x_k) in (3), (4), and (5) to $x - \varepsilon$.

Finally, one could require that the winner both exceed a threshold α *and* exceed all other signals by ε, that is,

$$X_k \geq X_j + \varepsilon \textit{ and } X_k \geq \alpha \text{ for all } k \neq j. \tag{10}$$

In this case the confusion matrix entries are found by setting all lower limits to α and all interior integral upper limits to $x - \varepsilon$ in (3), (4), and (5).

In summary then, *all* we need to know is the joint distribution $f_{Ti}(x, y, z,\ldots)$ or, if independence applies, $f_X(x)$, $f_Y(y)$, $f_Z(z),\ldots$, to *in principle* compute the conditional probabilities associated with the probability matrixes, regardless of whether the confusion matrices do or do not include a no-declare column. A later section will discuss the exact conditions required for independence.

III. TARGET REPRESENTATIONS

An HRR radar measures the radar return from various range bins along the length of a target. An RDI radar determines the returns from various range/cross-range bins.[3] Figure 4 shows a simplistic representation of the relative magnitudes of the radar energy returned by the scatterers associated with a hypothetical target for both RDI and HRR.[4] The two-dimensional pattern represents the results of the RDI measurements. The one-dimensional pattern at the bottom represents the cross-range sum of the relative intensity of all of the scatterers in a given range bin.[5] The two-dimensional pattern represented in Figure 4 contains 30 × 30 = 900 separate relative RCS measurements over a target. The assumed RCS values for each of these range/cross-range bins are not shown, but the 16-level color scale illustrates how the intensities vary across the target. The rectangular box of numbers in Figure 4 does show the cross-range sum of all of the RCS values in a range bin. The color bar at the bottom of the figure shows the relative intensities of the resulting one-dimensional profile, again on a 16-level color scale.[6]

We wish to represent the one-dimensional pattern of relative intensities as a vector called $\boldsymbol{S}_{1\mathrm{D}}$. That is, $\boldsymbol{S}_{1\mathrm{D}} = (2, 22, 4, \ldots, 2)^T$, where the superscript T indicates the transpose operation. In a similar manner, the relative intensities of the 900 two-dimensional returns could be recorded in a two-dimensional table, or they could just as easily be arranged in the form of a 900-element one-dimensional vector. For reasons that will become apparent shortly, we wish to represent two-dimensional targets using the latter form.

---

3 An RDI radar directly measures target returns in a polar pattern; interpolation is then required to generate a return pattern on a rectangular grid [2].

4 In reality, an actual target will likely have several scatterers within a given range or range/cross-range bin, so the radar return received for each radar bin will likely vary as the viewing geometry changes.

5 A straight summation of the radar cross section (RCS) associated with the various two-dimensional scatterers is also not totally correct, because there would be varying phase cancellation across a one-dimensional range bin as the viewing angle changes. This assumption is made at this point merely to facilitate the initial description of our approach.

6 The white regions represent the brightest regions in the two-dimensional and one-dimensional grids; however, these two-dimensional and one-dimensional white regions have different RCS values.

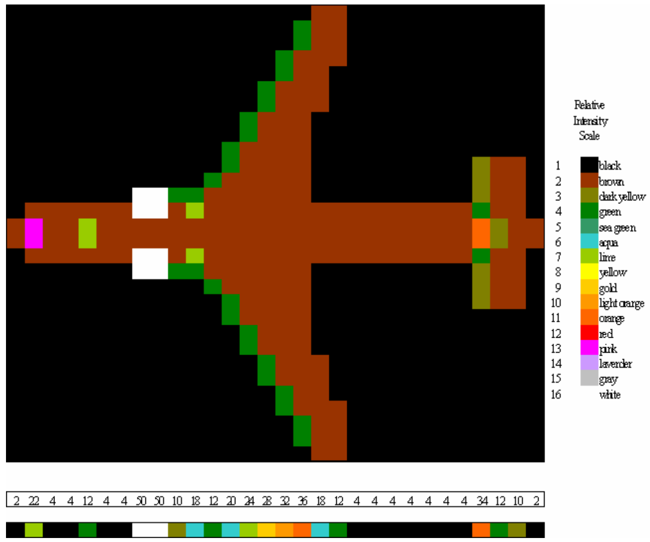

Figure 4. Simple Target Representation

Either the one-dimensional or two-dimensional target-characterization vectors could be normalized to one. Although not strictly necessary, we believe this normalization facilitates the analysis and helps in visualizing the computational process. Furthermore, normalization of the vectors will make the target templates (as defined by the one-dimensional or two-dimensional vectors) independent of the range between the radar and the target.

The foregoing discussion introduced the idea of representing a target as a one-dimensional or two-dimensional pattern of relative intensities or RCS values. Instead of reporting the relative RCS (or energy or signal power) for each of the bins, a radar could report the voltage associated with each bin. In reality, a radar will receive a waveform that contains both magnitude and phase. If the radar reports only the magnitude of the received signal, the elements of the target report vectors consist of a series of real, positive numbers. Alternatively, a series of complex numbers could be used to represent both the magnitude and phase of the received signal.

While an actual radar would measure the elements of the appropriate one-dimensional or two-dimensional vector, each component in the vector would include some noise, as follows:

$$\boldsymbol{Z} = \boldsymbol{S} + \boldsymbol{N} \tag{11}$$

where $\boldsymbol{Z}$ is the received signal recorded by the sensor, $\boldsymbol{S}$ is the vector of complex voltages received from the target when the noise is zero, and $\boldsymbol{N}$ is a noise vector of complex voltages that specifies the amount of noise added to each component of $\boldsymbol{S}$. We will make the standard simplifying assumption that all of the components of $\boldsymbol{N}$ are zero-mean, normally distributed random variables, and that each component has an identical standard deviation, σ, for both the real and imaginary parts of each component. Hence, the expected value of $\boldsymbol{Z}$ (which we denote as $< \boldsymbol{Z} >$) equals $\boldsymbol{S}$, and the covariance matrix of $\boldsymbol{Z}$ equals $2\,\sigma^2\boldsymbol{I}$, where $\boldsymbol{I}$ is the identity matrix with the number of rows and columns equal to the number of components in $\boldsymbol{Z}$. In mathematical notation:

$$< \boldsymbol{Z} > = \boldsymbol{S} \text{ and } < \boldsymbol{Z}\,\boldsymbol{Z}^H > - \boldsymbol{S}\,\boldsymbol{S}^H = 2\,\sigma^2\boldsymbol{I} = < \boldsymbol{N}\,\boldsymbol{N}^H > \tag{12}$$

where H indicates the Hermitian adjoint or conjugate transpose, since the elements of $\boldsymbol{Z}$ and $\boldsymbol{S}$ are assumed to be complex. The appendix (Section A-2b) provides proofs of these relationships. The factor of 2 appears in (12) because both the real and imaginary parts of each component of $\boldsymbol{N}$ are assumed to have a standard deviation of σ. It is easily shown (see Section A-3 and below) that the magnitudes of the components of the noise vector $\boldsymbol{N}$ have a Rayleigh distribution, and the magnitudes of components of the noisy target vector $\boldsymbol{Z}$ have a Rician distribution (see Section A-4).

IV. MATHEMATICAL PROCEDURES FOR TARGET RECOGNITION

As mentioned before, the ideal confusion matrix is the identity matrix (if the "no declare" column is eliminated). Therefore, one wants to maximize the probability of declaring that a target return indicates a target of type *X* when the underlying target is also of type *X*. Brennan and Reed [4] provided a matched filter formulation that maximizes the signal-to-noise ratio (SNR) when the actual target being observed, $\boldsymbol{Z}$ (where $\boldsymbol{Z} = \boldsymbol{S} + \boldsymbol{N}$), and the target template, $\boldsymbol{S}$, agree. Intuitively, this would seem to produce maximum values along the diagonal of the confusion matrix.[7] Brennan and Reed show that the maximum SNR obtainable for a target occurs when

$$\mathrm{SNR} = \mathrm{SNR}_{\max} = \boldsymbol{S}^H \boldsymbol{M}^{-1} \boldsymbol{S} \tag{13}$$

where $\boldsymbol{M}$ is the noise covariance matrix. For our assumed noise, see (12), $\boldsymbol{M} = 2\sigma^2 \boldsymbol{I}$. The inverse of $\boldsymbol{M}$ is $\boldsymbol{M}^{-1} = \boldsymbol{I} / (2\,\sigma^2)$. Considering only unit vectors (i.e., $|\boldsymbol{S}| = 1$), then $\mathrm{SNR}_{\max} = 1 / (2\sigma^2)$, since $\boldsymbol{S}^{\mathrm{H}}\boldsymbol{S} = 1$. For (13) to apply, the elements of the complex vector $\boldsymbol{S}$ must have units of voltage. The perceived SNR for an actual observation vector, $\boldsymbol{Z}_X = \boldsymbol{S}_X + \boldsymbol{N}$, against a test target, $\boldsymbol{S}_X$, becomes

$$SNR_{XX} = \boldsymbol{S}_X^H \boldsymbol{M}^{-1} \boldsymbol{Z}_X \tag{14}$$

where SNR_{XX} is a random variable, because $\boldsymbol{Z}_{\mathrm{X}}$ is a random variable. Likewise, when testing against template $\boldsymbol{S}_{\mathrm{T}}$, the expected value of SNR_{XT} is

$$< SNR_{XT} > = < \boldsymbol{S}_T^H \boldsymbol{M}^{-1} (\boldsymbol{S}_X + \boldsymbol{N}) > = \boldsymbol{S}_T^H \boldsymbol{S}_{\mathrm{X}} / (2\sigma^2) \tag{15}$$

because $< \boldsymbol{S}_T^H \boldsymbol{M}^{-1} \boldsymbol{N} > = \boldsymbol{S}_T^H \boldsymbol{M}^{-1} < \boldsymbol{N} > = 0$.

Figure 5 illustrates the application of (14) and (15). This figure represents the expected real and imaginary components of the complex values SNR_{XX} and SNR_{XT}. Because $\boldsymbol{S}_X^H\boldsymbol{S}_X = 1$, the expected value $< \boldsymbol{S}_X^H\boldsymbol{Z}_X >$ has real and imaginary components of 1 and 0, respectively. For a randomly chosen $\boldsymbol{Z}_X$, $\boldsymbol{S}_X^H\boldsymbol{Z}_X$ and $\boldsymbol{S}_T^H\boldsymbol{Z}_X$ will typically lie somewhere away from the expected positions of the phasors shown in Figure 5,

---

[7] Alternatively, one could view the problem as one of maximizing likelihood ratios and similarly calculate a decision statistic.

depending upon the value of σ. Figure 5 also illustrates two possible ways to determine whether $\boldsymbol{Z}_X$ better corresponds to either $\boldsymbol{S}_{\mathrm{X}}$ or $\boldsymbol{S}_{\mathrm{T}}$. In one case we compare the magnitudes using

$$|\boldsymbol{S}_X{}^H \boldsymbol{Z}_X| > |\boldsymbol{S}_T{}^H \boldsymbol{Z}_X|. \tag{16a}$$

In the other case we compare only the real parts using

$$\mathrm{Re}(\boldsymbol{S}_X{}^H \boldsymbol{Z}_X) > \mathrm{Re}(\boldsymbol{S}_T{}^H \boldsymbol{Z}_X). \tag{16b}$$

If the inequalities are satisfied, then one could conclude that $\boldsymbol{Z}_X$ more closely corresponds to $\boldsymbol{S}_{\mathrm{X}}$ than to $\boldsymbol{S}_{\mathrm{T}}$. From Figure 5, it appears that (16b) should outperform[8] (16a), although both should do well when the SNR is high, that is, $\sigma \to 0$. However, (16b) is sensitive to one's ability to determine the absolute phase of $\boldsymbol{Z}_X$. By absolute phase we mean determining the phase of the first component of the vector $\boldsymbol{Z}_X$ correctly and then determining the phase of all other components of $\boldsymbol{Z}_X$ relative to this first component. But when the SNR is low (and when the ability to make accurate discriminations is most desired), accurate absolute phase measurements become most difficult. In fact, if every component of the vector $\boldsymbol{Z}_X$ is rotated 180 deg due to an absolute phase measurement error, then the real-part-decision criterion would produce a reversed decision. On the other hand, the magnitude-comparison criterion would be unaffected by the absolute phase-measurement error. Therefore, in the remainder of this paper we will examine in detail the application of magnitude comparisons as defined by (16a).

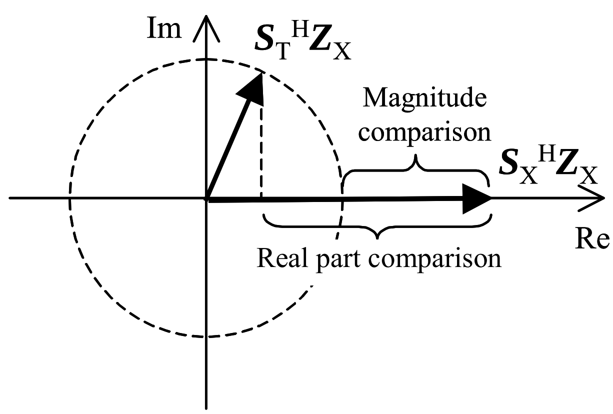

Figure 5. Depiction of Expected Values of Test Statistics in the Complex Plane and Possible Comparisons Between Them

---

8 As we were finalizing this paper, a colleague, Amnon Dalcher, pointed out that the real-part comparison is theoretically best when the inherent target magnitude is known while the absolute-value comparison is best when the inherent target magnitude is not known.

The foregoing reasoning gives the procedure for calculating the entries in a confusion matrix, namely:

- Assume a target of type i with template $\boldsymbol{S}_i$ such that $\boldsymbol{Z}_i = \boldsymbol{S}_i + \boldsymbol{N}$. This assumes that the true target template is known perfectly. This also assumes that $\boldsymbol{S}_{\mathrm{i}}^H\boldsymbol{S}_{\mathrm{i}} = 1$ such that $<|\boldsymbol{Z}_{\mathrm{i}}|> =1$. The impact of these assumptions could be explored by analyzing a number of real-world cases.
- Compute the inner (dot) product of $\boldsymbol{Z}_i$ with each of the possible target templates, $\boldsymbol{S}_j$, to form a test statistic $|T_{ij}| = |\boldsymbol{S}_j^H \boldsymbol{Z}_i|$, where $|T_{ij}|$ is a random variable. The test statistic involves a magnitude, since T_{ij} is generally a complex number.
- Determine the value of each confusion matrix entry by evaluating the probability expression $P(\text{declare } j \mid \text{target } i) = P(|T_{ij}| > |T_{i1}|, |T_{i2}|,\ldots, |T_{ik}|,\ldots)$ for all $k \neq j$.

Since the random vector $\boldsymbol{Z}_i$ appears in each of the random variables T_{ij}, there are cross correlations among the T_{ij}s. As a result, one would typically have to employ (3), instead of the more tractable (4) or (5). The degree to which the T_{ij}s (and hence the $|T_{ij}|$s) are correlated is found from the joint expectation of T_{ij} and T_{ik} or, more generally, the covariance matrix, defined by

$$C_{jk} = \left\langle (T_{ij} - < T_{ij} >)^* (T_{ik} - < T_{ik} >) \right\rangle . \tag{17}$$

In the appendix [see Section A-5, (A26)] it is shown that the covariance matrix is given by $C_{jk} = 2\sigma^2 \boldsymbol{S}_k^H \boldsymbol{S}_j$.[9] This implies there will be little correlation of the test statistics if the underlying target templates differ significantly (i.e., if $|\boldsymbol{S}_k^H \boldsymbol{S}_j| << 1$, except when $j = k$). The more orthogonal the target templates, the less risk one has in employing (4) or (5)—equations that assume statistical independence among all the test statistics.

[9] Note that the covariance matrix of the complex values T_{ij} does *not* depend on the true target $\boldsymbol{S}_i$. We later show, however, that the covariance matrix of the magnitudes $|T_{ij}|$ *does* depend on the true target.

V. EXAMPLE CASES

In this section, we present several example cases that illustrate the theoretical development outlined above. We begin with the coherent processing case even though in practice noncoherent processing is generally more predictable. The coherent case, especially when the targets are not correlated, yields a rather simple formulation. It also illustrates possible upper bounds, assuming one is able to measure the relative phase among the components of a target template. Our use of (16a), however, means that our coherent processing results do not require an absolute measurement of target phase; that is, our coherent process is insensitive to an absolute phase rotation of all elements in the measurement vector as might occur at low SNR when determining phase becomes especially difficult.

A. UNCORRELATED TARGETS—COHERENT PROCESSING

This case treats the ideal situation where all pairs of target templates have zero inner product (no overlap). Although this condition is not likely to occur in practice, we believe it is worthwhile to examine this case because the no-overlap condition could be approximately met in some cases. The independent target case also establishes the "best case" confusion matrix for a set of targets.[10] Let there be n mutually orthogonal targets denoted by $\boldsymbol{S}_i$, i = 1, 2,…, n. As in Chapter IV above, the test signal associated with target i is assumed to be $\boldsymbol{Z}_i = \boldsymbol{S}_i + \boldsymbol{N}$, where $\boldsymbol{N}$ is a complex, zero mean, Gaussian noise vector. Consider a given row i of the confusion matrix; this is the row associated with the true target $\boldsymbol{S}_i$. There are then n complex random variables of interest, given by $T_{ik} = \boldsymbol{S}_k^H \boldsymbol{Z}_i$, k = 1, 2,…, n. For notational clarity, in the remainder of this example we will suppress the true target subscript i, that is, $T_{ik} \rightarrow T_k$. Because the targets are orthogonal, the covariance matrix is diagonal, that is

$$C_{jk} = \left\langle (T_j - < T_j >)^* (T_k - < T_k >) \right\rangle = 2\sigma^2 \delta_{jk} \tag{18}$$

---

10 By best case, we mean the highest probability of correct target recognition for a given SNR.

and the random variables T_k are *independent*. Because the T_k are independent, their magnitudes, $R_k = |T_k|$, are also independent, with joint expectation [see Section A-4, (A27)] given by

$$<R_j R_k>= (1+2\sigma^2)\delta_{jk} \; . \tag{19}$$

Accordingly, the joint density of the R_ks factors,

$$f(R_1,R_2,...,R_n) = f_1(R_1)\, f_2(R_2)...\, f_n(R_n) \; . \tag{20}$$

All that is needed are expressions for the individual densities f_k on the right-hand side of (20). In the appendix (Section A-5) it is shown that for $k = i$ (if the template matches the true target), f_k is a Rician probability density; otherwise, f_k is a Rayleigh probability density,

$$f_k(R_k) = \begin{cases} \dfrac{R_k}{\sigma^2} e^{-\frac{(R_k{}^2+1)}{2\sigma^2}} I_0(\frac{R_k}{\sigma^2}), k = i \\ \dfrac{R_k}{\sigma^2} e^{-\frac{R_k{}^2}{2\sigma^2}} \qquad , k \neq i \end{cases} \; . \tag{21}$$

By applying (5), the confusion matrix entries for a given row can then be computed. We first recognize that neither PDF in (21) contains any parameters of the true target $\boldsymbol{S}_i$—only the noise parameter σ is present. It follows that one need only to compute the matrix elements for a single row. Further, from the structure of (5) it is clear that there are just two unique matrix elements: all $k = i$ (diagonal) elements are the same, and all $k \neq i$ (off-diagonal) elements are the same.[11] This makes sense intuitively because the mutual orthogonality of the targets prevents information from target i being gained by comparing it (dotting it) with target k. Finally, since the rows of the confusion matrix sum to one, and the off-diagonal elements are the same, the off-diagonal elements can be computed once the diagonal element is known. Therefore, there is just one integral to compute, the diagonal matrix element, given by

$$P_{\text{diag}} = \frac{1}{\sigma^{2n}} \int_0^\infty R e^{-\frac{(R^2+1)}{2\sigma^2}} I_0(\frac{R}{\sigma^2}) \left(\int_0^R u e^{-\frac{u^2}{2\sigma^2}} du \right)^{n-1} dR \tag{22a}$$

---

[11] This assumes square confusion matrices that do not contain a no-declare column. If a no-declare column were included, the limits in the ensuing integrals would have to be adjusted accordingly. Also, it assumes that the σs are all the same for each true target type, which may not always be a reasonable assumption, as discussed in Chapter VI.

$$= \sum_{k=0}^{n-1} \frac{(-1)^k (n-1)!}{(k+1)!(n-k-1)!} e^{-\frac{k}{2\sigma^2(k+1)}} \tag{22b}$$

which follows from (22a) by expanding the result of the interior integral as a binomial and applying the integral

$$\int_0^\infty R e^{-\alpha R^2} I_0(\beta R) dR = \tfrac{1}{2\alpha} e^{\frac{\beta^2}{4\alpha}} \tag{22c}$$

to the result [5]. The off-diagonal elements are given by the simple expression

$$P_{\text{off diag}} = \frac{1 - P_{\text{diag}}}{n-1} . \tag{23}$$

This yields the surprising result that the independent-target, coherent-processing case gives rise to a *universal* confusion matrix, whose elements are independent of the details of the individual targets.

Figure 6 shows a plot of the diagonal matrix element, (22), as a function of the SNR: SNR = $1/(2\sigma^2)$, for n = 2, 5, 10, and 20 targets. As the SNR approaches zero, P_{diag} approaches $1/n$; in this limit, the off-diagonal elements (23) equal the diagonal element, and there is equal probability of identifying *any one* of the targets as the true target. As the SNR increases, P_{diag} approaches one; correspondingly, the off-diagonal elements all approach zero.

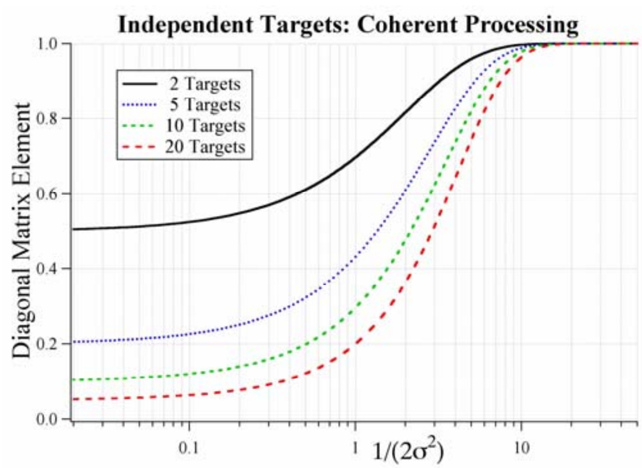

Figure 6. Diagonal Matrix Element as a Function of SNR for Independent Targets

B. CORRELATED TARGETS—COHERENT PROCESSING

In practice, there will always be overlap between targets.[12] For each true target $\boldsymbol{S}_i$, one is then confronted with a set of *n correlated* complex random variables $T_{ik} = \boldsymbol{S}_k^H \boldsymbol{Z}_i$, $k = 1, 2,\ldots, n$ with covariance matrix $C_{jk} = 2\sigma^2\ \boldsymbol{S}_k^H \boldsymbol{S}_j$ and the corresponding correlated magnitudes $R_{ik} = |T_{ik}|$. Here and throughout this section the true target subscript i is retained. To compute confusion-matrix entries, one must use the general probability relation given in (3); however, a prerequisite is the joint PDF of the magnitudes, $f_i(R_{i1}, R_{i2},\ldots, R_{in})$. We show in the appendix [Section A-5, (A33)] that the PDF for each amplitude R_{ik} is given by the Rician density

$$f_{ik}(R_{ik}) = \frac{R_{ik}}{\sigma^2} e^{-\frac{(R_{ik}{}^2 + c_{ik}{}^2)}{2\sigma^2}} I_0\left(\tfrac{R_{ik}c_{ik}}{\sigma^2}\right) \tag{24}$$

where c_{ik}=| $\boldsymbol{S}_k^H \boldsymbol{S}_i$ |. To construct the exact joint PDF of the correlated Rician random variables, the second-order correlations, $<R_{ij}\ R_{ik}>$, *and all higher order correlations* are needed. Unfortunately, to our knowledge, neither these correlations, nor the joint PDF itself, can be computed in closed form [6].

In spite of this, an approximate joint PDF can be constructed in the high signal-to-noise limit (i.e., when σ/c_{ik} <<1). In this limit, the Rician PDFs in (24) are well approximated by Gaussian PDFs (see Section A-4 for justification), and the joint PDF is well approximated by a multidimensional Gaussian of the form [7]

$$\begin{aligned} f_i(\boldsymbol{R}_i) \approx & \frac{1}{\sqrt{(2\pi)^n \det(K_i)}} \\ & \exp(-\tfrac{1}{2}(\boldsymbol{R}_i - \mu_i)^T K_i^{-1}(\boldsymbol{R}_i - \mu_i)) \end{aligned} \tag{25}$$

where $\boldsymbol{R}_i \equiv (R_{i1}, R_{i2},\ldots,R_{in})^T$, $\mu_i = \langle \boldsymbol{R}_i \rangle$, and K_i is the covariance matrix of the amplitudes. The components of the mean vector can be computed exactly from the mean of a Rician random variable (see Section A-4):

$$< R_{ik} >= \tfrac{\sigma}{2}\sqrt{\tfrac{\pi}{2}}\, e^{-\frac{c_{ik}{}^2}{4\sigma^2}} \left[(2 + \tfrac{c_{ik}{}^2}{\sigma^2}) I_0(\tfrac{c_{ik}{}^2}{4\sigma^2}) + \tfrac{c_{ik}{}^2}{\sigma^2} I_1(\tfrac{c_{ik}{}^2}{4\sigma^2}) \right] \tag{26}$$

where I_0 and I_1 are the zeroth and first-order modified Bessel functions of the first kind.

The elements of the covariance matrix for true target $\boldsymbol{S}_i$ are given by

$$K_{jk}(i) \equiv \left\langle (R_{ij} - < R_{ij} >)(R_{ik} - < R_{ik} >) \right\rangle = < R_{ij}R_{ik} > - < R_{ij} >< R_{ik} > . \tag{27}$$

---

[12] A judicious choice of target vectors could conceivably help reduce the overlap between targets, however. This topic is taken up in Chapter VI.

The diagonal (j = k) elements of the joint expectation of R_{ij} and R_{ik} can be computed exactly [see (A21)]:

$$< R_{ij}^2 >= c_{ij}^2 + 2\sigma^2 . \tag{28}$$

Although it is not possible, to our knowledge, to compute the off-diagonal elements of the joint expectation of R_{ij} and R_{ik} exactly, a lengthy but straightforward calculation (see Section A-5) shows that to order σ^2, the joint expectation is given by

$$< R_{ij} R_{ik} > \approx c_{ij} c_{ik} + \frac{\sigma^2}{2 c_{ij} c_{ik}} \left(c_{ij}^2 + c_{ik}^2 + 2 c_{ij} c_{ik} c_{kj} \cos(\phi_{ij} - \phi_{ik} - \phi_{kj}) \right) \tag{29}$$

where the phases are defined though the relations $\boldsymbol{S}_j^H \boldsymbol{S}_i = c_{ij} e^{i\phi_{ij}}$, $\boldsymbol{S}_k^H \boldsymbol{S}_i = c_{ik} e^{i\phi_{ik}}$, and $\boldsymbol{S}_j^H \boldsymbol{S}_k = c_{kj} e^{i\phi_{kj}}$.[13] With the mean and covariance in hand, the confusion matrix entries for high signal to noise can be estimated by numerically integrating (3), using the joint PDF (25), repeated here using the notation of this section:

$$P(\boldsymbol{S}_j \mid \boldsymbol{S}_i) = \int_{-\infty}^{\infty} dR_{ij} \left(\prod_{\substack{k=1 \\ k \neq j}}^{n} \int_{-\infty}^{R_{ij}} dR_{ik} \right) f_i(\boldsymbol{R}_i) . \tag{30}$$

We give here an example with the simplest possible case of two targets, $\boldsymbol{S}_1$ and $\boldsymbol{S}_2$. This case leads to several simplifications. First, there is only a single off-diagonal element in the covariance matrix (27). Further, the joint expectation (29), and therefore the covariance matrix (27), does not depend on the phases. For true target $\boldsymbol{S}_1$ (i = 1) (29), reduces to

$$< R_{11} R_{12} >= c_{12} + \frac{\sigma^2}{2 c_{12}} \left(1 + 3 c_{12}^2 \right) \tag{31}$$

again valid to order σ^2. An expression for the mean of a Rician in the high SNR limit is derived in the appendix. Applying this expression to R_{11} and R_{12} yields

$$< R_{11} >= 1 + \frac{\sigma^2}{2} \tag{32a}$$

$$< R_{12} >= c_{12} + \frac{\sigma^2}{2 c_{12}} . \tag{32b}$$

By combining (27), (28), (31), and (32) and simplifying, we arrive at a simple approximate expression for the covariance matrix associated with true target $\boldsymbol{S}_1$:

---

[13] Note that for $j = k$ (diagonal elements), expression (29) is *exact* and reduces to the result in (28).

$$K_1 = \begin{bmatrix} \sigma^2(1-\frac{\sigma^2}{4}) & c_{12}\sigma^2(1-\frac{\sigma^2}{4c_{12}^2}) \\ c_{12}\sigma^2(1-\frac{\sigma^2}{4c_{12}^2}) & \sigma^2(1-\frac{\sigma^2}{4c_{12}^2}) \end{bmatrix}. \tag{33}$$

It is evident that the covariance matrix, K_2, associated with target $\boldsymbol{S}_2$, is obtained by interchanging the diagonal elements of K_1. Because of the symmetry of the two-target case, the diagonal elements of the confusion matrix are identical, as are the off-diagonal elements. Within the Gaussian approximation, there are then just two parameters that define the two-target case—the magnitude of the target correlation, $c_{12}=|\ \boldsymbol{S}_2^H\boldsymbol{S}_1\ |$, and the noise strength σ.[14]

Figure 7 shows the diagonal element of the two-target case, that is, the probability of correct target identification, computed from the Gaussian approximation (30), as a function of SNR = $1/(2\sigma^2)$ for four values of the target correlation: c_{12} = 0.3, 0.5, 0.7, and 0.9. For comparison, the independent target result, (22), is also shown. Also plotted are *simulated* results for two two-dimensional complex templates with correlations 0.3, 0.5, 0.7, and 0.9.[15] Simulations were performed by sampling the signal vector 100 000 times, projecting each onto the 2 templates vectors, and computing the fraction of cases when one projection exceeds the other. The agreement between the Gaussian approximation and simulated results is seen to improve with increasing SNR and for increasing correlation. Because the Gaussian approximation holds only for high SNR, the Gaussian approximation curves in Figure 7 are limited to SNR values that correspond to the condition $\sigma/c_{12} < 1.5$. It is apparent from the figure that the probability of correct target ID diminishes with increasing target correlation and that a high degree of target correlation (e.g., c_{12} = 0.9) degrades the probability significantly from the independent target result (roughly 20 percent for an SNR = 10).

---

14 It can be shown that the two-target case depends only on c_{12} and σ for the entire range of SNR values.

15 The template vectors were taken to be $\boldsymbol{S}_1 = \frac{1}{\sqrt{2}}\begin{pmatrix}1\\1\end{pmatrix}$ and $\boldsymbol{S}_2 = \begin{pmatrix}\alpha\\ \sqrt{1-\alpha^2}\,e^{i\theta}\end{pmatrix}$. Overlap values of 0.3, 0.5, 0.7, and 0.9 can be obtained with parameter pairs (α, θ) = (0.4756, 2.9413), (0.2645, 2.9413), (0.0102, 2.9413), and (0.7071, 0.9021), respectively.

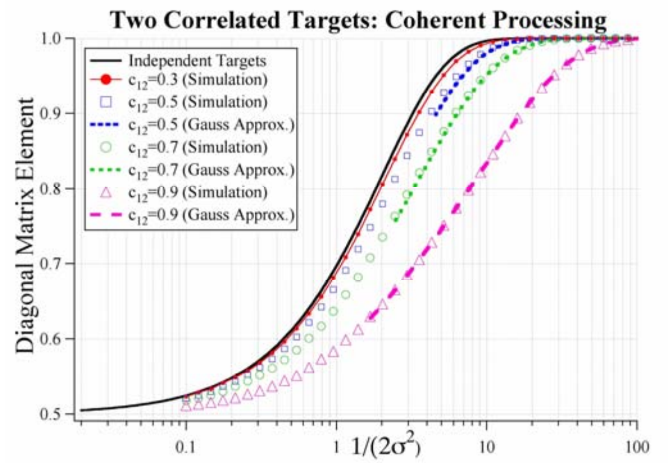

Figure 7. Diagonal Matrix Element as a Function of SNR for Two Correlated Targets

C. CORRELATED TARGETS—NONCOHERENT PROCESSING

An alternative approach to the coherent processing case is to represent all target templates as *real* vectors by retaining only the magnitudes of the components of the normalized complex templates $\boldsymbol{S}_i$ above. The real template vectors are denoted by

$$\boldsymbol{A}_i = (a_{i1}, a_{i2}, \ldots, a_{im})^T = (|s_{i1}|, |s_{i2}|, \ldots, |s_{im}|)^T ,$$

$$i = 1, 2, \ldots, n, \tag{34}$$

where m is the number of components of $\boldsymbol{S}_i$. Since the $\boldsymbol{S}_i$ are normalized according to $\boldsymbol{S}_i^H \boldsymbol{S}_i = 1$, the $\boldsymbol{A}_i$ are automatically normalized according to $\boldsymbol{A}_i^T \boldsymbol{A}_i = 1$.

Similarly, signal vectors are represented by vectors whose components are the magnitudes of the components of the complex vector $\boldsymbol{Z}_i = \boldsymbol{S}_i + \boldsymbol{N}$. Hence, signal vectors are represented by

$$\begin{aligned} \boldsymbol{Y}_i &= (y_{i1}, y_{i2}, \ldots, y_{im})^T \\ &= (|s_{i1} + n_1|, |s_{i2} + n_2|, \ldots, |s_{im} + n_m|)^T \end{aligned}$$

$$i = 1, 2, \ldots, n. \tag{35}$$

In radar parlance, this is known as noncoherent processing. As discussed previously, *each component* of $\boldsymbol{Y}_i$ is a Rician random variable with PDF

$$f_{ik}(y_{ik}) = \frac{y_{ik}}{\sigma^2} e^{-\frac{(y_{ik}{}^2 + a_{ik}{}^2)}{2\sigma^2}} I_0\left(\tfrac{y_{ik} a_{ik}}{\sigma^2}\right) \ . \tag{36}$$

To compare template $\boldsymbol{A}_k$ with true target $\boldsymbol{Y}_i$, we form the inner product[16]

$$w_{ik} = \boldsymbol{A}_k{}^T \boldsymbol{Y}_i = \sum_{\alpha=1}^{m} a_{k\alpha} y_{i\alpha} \quad . \tag{37}$$

For each true target, we are again confronted with a set of n correlated random variables w_{ik}, $k = 1, 2, \ldots, n$. Again, the joint PDF is desired, but it is impossible to compute in closed form. An approximate method for obtaining the joint PDF is presented in the following. Since each component of $\boldsymbol{Y}_i$ is a Rician[17] random variable, w_{ik} is a strictly positive weighted sum of Rician random variables. By the central-limit theorem, as the number of components, m, of $\boldsymbol{Y}_i$ increases, the density function of w_{ik} approaches a Gaussian. Similar to the coherent case above, we again seek a joint PDF in terms of a multidimensional Gaussian

$$f_i(\boldsymbol{w}_i) = \frac{1}{\sqrt{(2\pi)^n \det(Q_i)}} \cdot \exp(-\tfrac{1}{2}(\boldsymbol{w}_i - \zeta_i)^T Q_i^{-1} (\boldsymbol{w}_i - \zeta_i)) \tag{38}$$

where $\boldsymbol{w}_i = (w_{i1}, w_{i2}, \ldots, w_{in})^T$, $\zeta_i = <\boldsymbol{w}_i>$, and Q_i is the covariance matrix for the random variables w_{ik}. The mean vector ζ_i can be computed exactly with the help of (26). In the appendix [Section A-6, (A55)] we show that the covariance matrix Q_i can be computed exactly:

$$Q_{jk}(i) \equiv <(w_{ij} - <w_{ij}>)(w_{ik} - <w_{ik}>)> = \sum_{\alpha=1}^{m} a_{j\alpha} \sigma_{i\alpha}^2 a_{k\alpha} \tag{39}$$

where $\sigma_{i\alpha}^2 = <y_{i\alpha}^2> - <y_{i\alpha}>^2$ is the variance of the Rician random variable $y_{i\alpha}$, an expression for which is given in the appendix (Section A-4). Finally, the confusion matrix entries can be found by employing the general probability expression in (3). Note that each true target $\boldsymbol{A}_i$ (i^{th} row) is associated with a distinct joint density f_i. We proceed with a numerical example to illustrate the method.

Figure 8 shows images of three target templates, fashioned to resemble simple plan views of three (admittedly bizarre) aircraft. The targets are represented by 4×5 matrices, given by

---

16 We will first follow the same recipe as just developed for the coherent case. However, we will then demonstrate that some difficulties can arise at low SNR values. These difficulties ultimately lead to an alternative formulation that eliminates the low-SNR problems.

17 Some of the terms in $\boldsymbol{Y}_{\mathrm{i}}$ will correspond to Rayleigh random variables, but the Rayleigh is merely a special case of the Rician.

$$\boldsymbol{A}_1 = \frac{1}{\sqrt{10}}\begin{pmatrix} 0 & 1 & 1 & 1 & 0 \\ 0 & 0 & 1 & 0 & 0 \\ 1 & 1 & 1 & 1 & 1 \\ 0 & 0 & 1 & 0 & 0 \end{pmatrix}, \boldsymbol{A}_2 = \frac{1}{\sqrt{10}}\begin{pmatrix} 1 & 1 & 0 & 1 & 1 \\ 0 & 0 & 1 & 0 & 0 \\ 1 & 1 & 0 & 1 & 1 \\ 0 & 0 & 1 & 0 & 0 \end{pmatrix}, \boldsymbol{A}_3 = \frac{1}{\sqrt{18}}\begin{pmatrix} 0 & 0 & 0 & 0 & 0 \\ 2 & 2 & 1 & 2 & 2 \\ 0 & 0 & 1 & 0 & 0 \\ 0 & 0 & 0 & 0 & 0 \end{pmatrix}. \quad (40)$$

Figure 8. Three Hypothetical Templates Represented by Matrices in (40)

The lighter shading in the figure represents the larger matrix entries. Each template can be recast as a 20-dimensional vector. The matrix of inner products between all templates is then given by

$$\begin{pmatrix} \boldsymbol{A}_1^T\boldsymbol{A}_1 & \boldsymbol{A}_1^T\boldsymbol{A}_2 & \boldsymbol{A}_1^T\boldsymbol{A}_3 \\ \boldsymbol{A}_2^T\boldsymbol{A}_1 & \boldsymbol{A}_2^T\boldsymbol{A}_2 & \boldsymbol{A}_2^T\boldsymbol{A}_3 \\ \boldsymbol{A}_3^T\boldsymbol{A}_1 & \boldsymbol{A}_3^T\boldsymbol{A}_2 & \boldsymbol{A}_3^T\boldsymbol{A}_3 \end{pmatrix} = \begin{pmatrix} 1 & 0.8 & 0.149 \\ 0.8 & 1 & 0.0745 \\ 0.149 & 0.0745 & 1 \end{pmatrix}. \quad (41)$$

Consistent with Figure 8, there is significant overlap between targets 1 and 2, less overlap between targets 1 and 3, and very little overlap between targets 2 and 3.

We first examine pairwise target comparisons, starting with targets 1 and 2 in Figure 8. Figure 9 shows a plot of the matrix element P_{11} of the 2×2 confusion matrix as a function of SNR = $1/(2\sigma^2)$, both with the Gaussian approximation in (38) (solid) and with direct simulation (open circles). Simulations were performed by sampling the signal vector, with $\boldsymbol{A}_1$ as the true target, 100 000 times, projecting each onto the two templates vectors $\boldsymbol{A}_1$ and $\boldsymbol{A}_2$, and computing the fraction of cases when one projection exceeds the other. The good agreement between the Gaussian approximation and simulated results justifies the use of the Gaussian approximation for these 20-dimensional target templates. The matrix element P_{22} exhibits essentially identical behavior; good agreement between the Gaussian approximation and the simulated results is also observed. Shown for comparison in Figure 9 is the simulated two-target coherent case with an overlap of 0.8. As expected, the coherent result outperforms the noncoherent result, particularly for low SNRs.

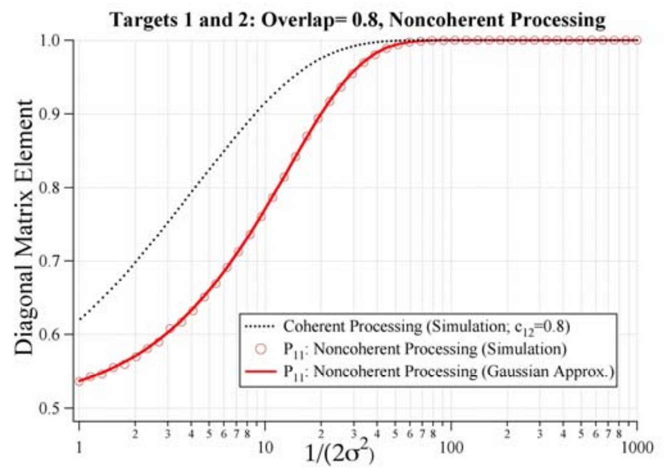

Figure 9. P_{11} **vs. SNR for Pairwise Comparison of Targets 1 and 2 in Figure 8**

Figure 10 shows the confusion matrix elements P_{11} and P_{33} as a function of SNR for the pairwise comparison of targets 1 and 3 shown in Figure 8. Displayed in the plot are the confusion matrix elements computed with the Gaussian approximation and with direct simulation, as in the creation of Figure 9. Again, the Gaussian approximation is seen to agree well with the simulated results. Also shown is the simulated two-target coherent case for an overlap of 0.15. Unfortunately, the noncoherent results in Figure 10 make no sense. At very low SNR values, one would expect that targets 1 and 3 would be indistinguishable and each would be selected with a 50-percent probability when choosing only between these two targets.

The explanation for this behavior is as follows. It is shown in the appendix (A19) that for small A/σ (low SNR), the mean of a Rician approaches $\sigma\sqrt{\frac{\pi}{2}}$ (this is the mean of a Rayleigh random variable). Therefore, the expected measured-signal vector approaches $\sigma\sqrt{\frac{\pi}{2}}\ (1,1,\ldots,1)^T$. It follows from the definition of w_{ik} in (37) that the template $\boldsymbol{A}_k$, whose components sum to the largest value, will yield the largest projection (alternatively, the template that "looks" most like the $(1,1,1,\ldots,1)^T$ vector "wins"). Consequently, the probabilities associated with this template will be skewed to larger values. In the case of targets 1 and 3, the component sums are $\sqrt{10} = 3.16$ and $10/\sqrt{18} = 2.36$. This explains why, in Figure 10, as SNR decreases, P_{11} is abnormally large and P_{33} is abnormally small. In each case the projection onto target 1 is consistently larger than the projection onto target 3. *We emphasize that this effect is a natural consequence of applying the projection methodology to noncoherent processing—it is* not *an artifact of the Gaussian approximation technique outlined above.* Similar results are observed when targets 2 and 3 are compared, with target 2 "winning" as the SNR decreases (the component sum for target 2 is the same as for target 1).

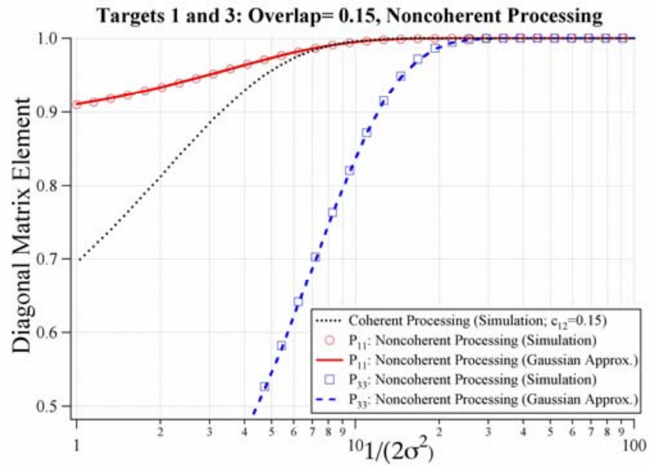

Figure 10. P_{11} **and** P_{33} **vs. SNR Pairwise Comparison of Targets 1 and 3 in Figure 8 Demonstrates a Flaw in our Direct Use of a Linear Process**

Although the foregoing discussion explains why the bizarre result depicted in Figure 10 occurs, this limitation seems rather unsatisfying. Therefore, upon further reflection, we realized that the problem actually lay in our representation of the target templates.[18] We really need to define target templates that represent the *expected return* when observing a target.[19] Hence the target templates for the noncoherent case need to be defined as follows:

$$\boldsymbol{A}_j = \left(<\left|s_{j1}+n_1\right|>,<\left|s_{j2}+n_2\right|>,\ldots,<\left|s_{jm}+n_m\right|>\right)^T . \tag{42}$$

The terms in (42) are the means of Rician processes such that $<|s_{jk} + n_k|> = f(s_{jk}, n_k) > s_{jk}$, where $f(s_{jk}, n_k)$ indicates that the mean of a Rician process is a function of both the signal s_{jk} and the noise n_k. For large SNR, $<|s_{jk} + n_k|> \longrightarrow s_{jk}$, and for small SNR, $<|s_{jk} + n_k|> = \sqrt{\pi/2}\,\sigma$. Obviously, this means that the target templates must vary with SNR. The appendix (Section A-4) shows how to calculate exactly the means of the Rician random variables. While we have used this exact calculation in developing the ensuing illustration, a reasonable numerical approximation we have empirically derived (i.e., within ~ 1 percent) is as follows:

$$<\left|s_{jk}+n_k\right|>\approx\left[\left(s_{jk}\right)^{2.25}+\left(\sqrt{\pi/2}\,\sigma_k\right)^{2.25}\right]^{\left(1/2.25\right)} . \tag{43}$$

---

18 An analogous issue occurs in noncoherent detection theory, which uses a square law, as opposed to a linear, detector when the SNR is low.

19 Without directly thinking about it this way, that is exactly what occurs in the coherent case because the noise is zero-mean Gaussian.

Based on these considerations, the target 1 and 3 templates for SNR values of 1, 4, and 10 are shown in Table I.

Table I. SNR-Dependent Noncoherent Target Templates

Target 1 Templates	Target 3 Templates
SNR = 1	
$\begin{pmatrix} 0.886 & 0.930 & 0.930 & 0.930 & 0.886 \\ 0.886 & 0.886 & 0.930 & 0.886 & 0.886 \\ 0.930 & 0.930 & 0.930 & 0.930 & 0.930 \\ 0.886 & 0.886 & 0.930 & 0.886 & 0.886 \end{pmatrix}$	$\begin{pmatrix} 0.886 & 0.886 & 0.886 & 0.886 & 0.886 \\ 0.982 & 0.982 & 0.911 & 0.982 & 0.982 \\ 0.886 & 0.886 & 0.911 & 0.886 & 0.886 \\ 0.886 & 0.886 & 0.886 & 0.886 & 0.886 \end{pmatrix}$
SNR = 4	
$\begin{pmatrix} 0.443 & 0.528 & 0.528 & 0.528 & 0.443 \\ 0.443 & 0.443 & 0.528 & 0.443 & 0.443 \\ 0.528 & 0.528 & 0.528 & 0.528 & 0.528 \\ 0.443 & 0.443 & 0.528 & 0.443 & 0.443 \end{pmatrix}$	$\begin{pmatrix} 0.443 & 0.443 & 0.443 & 0.443 & 0.443 \\ 0.621 & 0.621 & 0.491 & 0.621 & 0.621 \\ 0.443 & 0.443 & 0.491 & 0.443 & 0.443 \\ 0.443 & 0.443 & 0.443 & 0.443 & 0.443 \end{pmatrix}$
SNR = 10	
$\begin{pmatrix} 0.280 & 0.405 & 0.405 & 0.405 & 0.280 \\ 0.280 & 0.280 & 0.405 & 0.280 & 0.280 \\ 0.405 & 0.405 & 0.405 & 0.405 & 0.405 \\ 0.280 & 0.280 & 0.405 & 0.280 & 0.280 \end{pmatrix}$	$\begin{pmatrix} 0.280 & 0.280 & 0.280 & 0.280 & 0.280 \\ 0.529 & 0.529 & 0.353 & 0.529 & 0.529 \\ 0.280 & 0.280 & 0.353 & 0.280 & 0.280 \\ 0.280 & 0.280 & 0.280 & 0.280 & 0.280 \end{pmatrix}$

When processing variable target templates such as these using (37), one obtains the results shown in Figure 11. As before, the simulated results come from averaging the results of 100 000 trials at each SNR value.

Using this revised template definition process, Figure 11 shows that the decision between targets 1 and 3 becomes 50–50 at low SNR values. Also, the results parallel, but fall below, the curve obtained for coherent processing with a target template correlation of 0.15. Although the above method will work when developing confusion-matrix probabilities for noncoherent processing, the practical implementation of these SNR-dependent templates will necessitate estimating the noise. This could be accomplished by averaging the returns for elements of the original template where the RCS is zero (e.g., elements outside the extent of the target). In these regions, the Rayleigh distribution applies, and the value of the noise parameter can be observed directly.

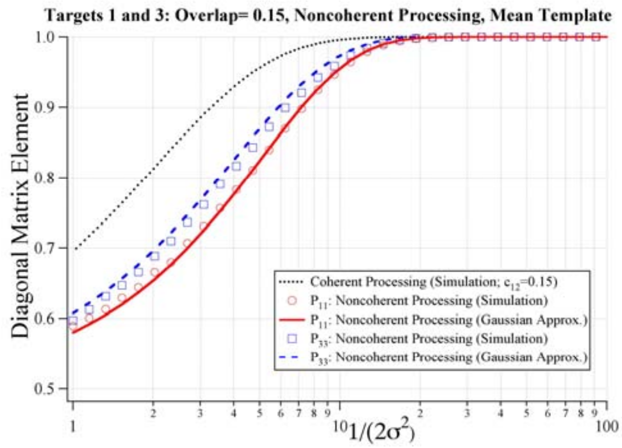

Figure 11. Corrected Results of P_{11} and P_{33} vs. SNR with Revised Templates for Targets 1 and 3

VI. PRACTICAL CONSIDERATIONS

This section discusses a few practical issues associated with implementing the computations discussed above.

A. UNCERTAINTIES ASSOCIATED WITH COHERENT PROCESSING

Section V began with a discussion of a target-processing scheme that involved target template and measurement vectors that contain complex terms to represent the relative phase between positions in the vectors. Although magnitude processing is insensitive to absolute phase-measurement errors, it still requires extremely precise knowledge of the viewing angle of the target, as well as significant uniformity among the various actual targets being represented by a target template vector. Neither of these conditions will consistently occur in practice. For example, if one considers the two-scatterer situation depicted in Figure 12, then the relative phase between a return from each of the individual scatters varies as follows:

$$\begin{aligned}\Delta\Phi &= \omega\,\Delta t = \omega\frac{2\,\Delta d}{c} = \frac{2\,\omega\,N\,\lambda\left(1-\cos\Theta\right)}{\omega\lambda/2\pi} \\ &= 4\pi N\left(1-\cos\Theta\right)\end{aligned} \quad . \tag{44}$$

$$\frac{d\Delta\Phi}{d\Theta} = 4\pi N\sin\Theta \,. \tag{45}$$

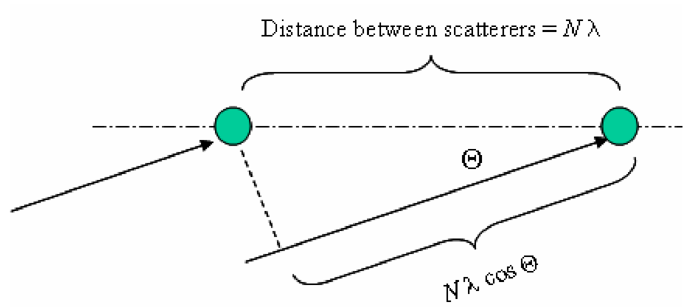

Figure 12. Longitudinal Phase Difference Geometry

For example, for two scatters separated by 1 meter at X band (10^{10} Hz), N = 100/3, so the variation in Φ as Θ varies approximately equals 420 Θ when the angle Θ is small. Hence, even a small uncertainty in the viewing angle Θ results in a large change in the relative phase, even though the apparent difference in the relative positions of the scatters would be imperceptible.

B. TARGET SCINTILLATION EFFECTS

If a range bin contains multiple scatterers, then the received HRR signal will vary as the viewing angle changes. Figure 13 shows the simplest case of only two scatterers in the same range bin separated by a distance of $n\lambda$. With respect to the centroid of the two scatterers, the relative phase from the individual scatterers is given by

$$\Delta\Phi = \omega\,\Delta t = \omega\frac{2\,\Delta d}{c} = 2\,\omega\frac{(n\lambda/2)\sin\Theta}{\omega\,\lambda/2\pi} = 2\pi\,n\,\sin\Theta \approx 2\pi\,n\,\Theta \qquad (46)$$

so the received signal becomes

$$\sin(\omega t + \Delta\Phi) + \sin(\omega t - \Delta\Phi) = [2\cos(2\pi n\Theta)]\sin\omega t\ . \qquad (47)$$

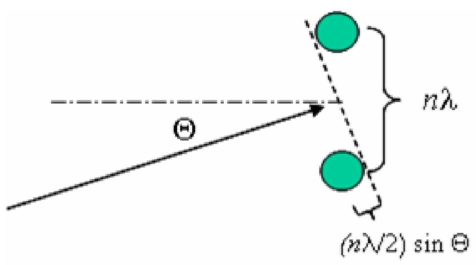

Figure 13. Scintillation Geometry

At X band for this simple case of two scatterers in the same range bin separated vertically by 1 meter, the amplitude of the received signal varies with angle as shown in Figure 14. The amplitude of the sine term in (47) depends greatly on the angle Θ. However, if two range bins separated longitudinally by an arbitrary distance happen to both have two scatterers separated by 1 meter, then the relative difference in magnitude between these two range bins would not vary with the angle Θ. Of course, as the amplitudes approach zero (i.e., $[2\cos(2\pi n\Theta)] \rightarrow 0$), one's ability to recognize that the returns are equal will disappear as noise becomes comparable in magnitude to the signal.

C. EFFECT OF TOTAL TARGET RETURN ON NOISE VALUES

The above analyses assumed unit target template vectors (i.e., $\boldsymbol{S}_X^H\boldsymbol{S}_X = 1$). This was done so the relative angles between the template vectors would provide a direct measure of the degree of independence between the individual target templates. However, this also means that all the target templates used in building the confusion

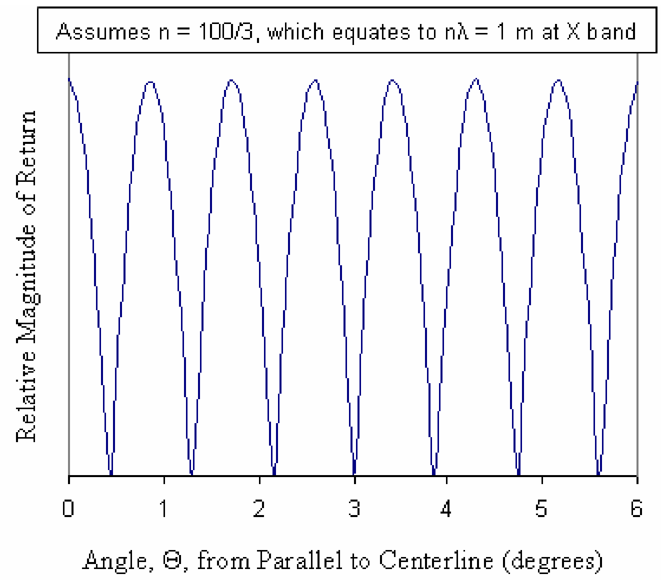

Figure 14. Variation in Magnitude of Return as Angle Changes

matrices assume that all targets are equally bright (or dim). This effect matters most when thinking about the various rows in the confusion matrix that correspond to a priori assumptions that each of the various targets is being observed. In reality, there can be substantial variability in the total brightness of targets (e.g., transport aircraft vs. cruise missiles). When making a target observation, we will observe $\boldsymbol{Z}_X$, where $\boldsymbol{Z}_X = \boldsymbol{T}_X + \boldsymbol{N}$. While we can compute $|\boldsymbol{Z}_X|$ directly, we would really like to determine $|\boldsymbol{T}_X|$. However, if we can estimate the amount of noise (which we might do by observing returns in components of $\boldsymbol{Z}_X$ without any target signal present), then we could estimate $|\boldsymbol{T}_X|$. With this we could then form

$$\boldsymbol{Z}'_X = \frac{\boldsymbol{T}_X + \boldsymbol{N}}{|\boldsymbol{T}_X|} = \boldsymbol{S}_X + \frac{\boldsymbol{N}}{|\boldsymbol{T}_X|} \tag{48}$$

where $\boldsymbol{S}_X$ is now the unit target template. From (48) we see that the noise portion of $\boldsymbol{Z}'_X$ varies with the brightness of the target. As the magnitude of the noise varies, the entries in the confusion matrices vary (e.g., see Figure 7 or 11). The details of how to address this effect are outside the scope of the material we wish to address in this paper.

D. EVALUATION OF TARGET CLASSES AND TARGET FLUCTUATIONS

The above formulations have considered that each target will have a unique target template. However, situations might arise such as the one depicted in Figure 15, in which groups of targets appear highly correlated, but the correlation between the target groups is small. For example, one target group could involve two-engine fighter aircraft (e.g., F-

15, F-18, Mig-29) while another could involve two-engine commercial aircraft (e.g., B-757, B-767, A-310). In this case, one could form a composite template for each of the target groups and then compare measured targets against each of the groups. A simple way to do this would be to assume increased noise associated with the target measurements so as to include both the actual noise and a dispersion-effect noise that addresses the variation among targets within a given class, as shown in Figure 16.[20] A subset of this problem might involve grouping the various models (e.g., F-15C, F-15E) or configurations (e.g., with or without stores) of an aircraft into a composite aircraft category (e.g., F-15). This would likely result in less dispersion within such a generic airframe category than would occur across a broader class of, say, all two-engine fighters. The actual or synthesized target template data and the variations in the individual target template dot products among the various targets will have to be examined to determine which target groupings make most sense.

In a similar manner to that shown in Figure 16, one could increase the values for the terms in the target's covariance matrix to account for target fluctuations. In this case the terms in the noise covariance matrix would correspond to the sum of the squares of standard deviations for both the inherent system noise (e.g., thermal noise) and the target fluctuations.

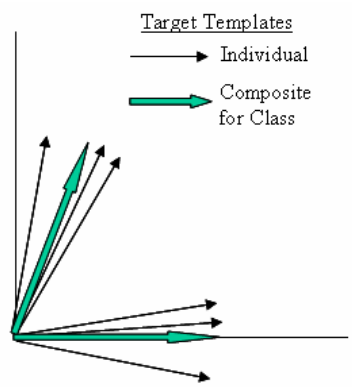

Figure 15. Formation of Target Class Templates

[20] Because there will typically be fewer targets in a class than components in the template vectors, the effective noise for the class will no longer appear as a hyper-sphere (despite the depiction in Figure 15). Hence the noise covariance matrix associated with the target class will become a hyper-ellipse, which would necessitate modifications to the formulations shown in Chapter V, beginning with (18).

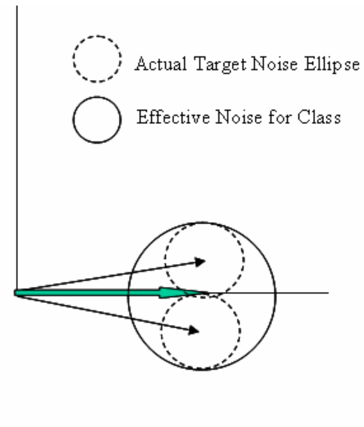

Figure 16. "Noise" for Target Class

E. EVALUATION OF NON-ISOTROPIC NOISE

When the noise covariance is non-isotropic, the results presented in Section 5 require modification. The noise could be non-isotropic because the nominal target is a composite of a number of similar targets, as just illustrated in Figure 15, or due to the use of noncoherent processing. For example, with noncoherent processing when the target template is $(1, 0)^T$ and the SNR equals 1, the expected template is $(1.545, 1.253)^T$ and the corresponding standard deviations are 0.783 and 0.655. So clearly noncoherent processing can lead to ellipsoidal rather than spherical noise matrices. Figure 17 shows a generic depiction of this situation.

The test statistic (14) includes a noise covariance matrix that will therefore adjust for non-isotropic noise. The Fisher Linear Discriminant [8] provides an alternative way to think about the problem. It allows one to determine the maximum separation between two data sets based on the separation between the means of the two populations and the combined covariance of the two populations. The Fisher Linear Discriminant is given by:

$$\boldsymbol{V}_s = C_c^{-1}\left(\boldsymbol{m}_1 - \boldsymbol{m}_2\right) \tag{49}$$

where:

$\boldsymbol{V}_s$ is the vector for maximum statistical separation

$C_c^{-1} = \mathrm{Inv}(C_c)$ where $C_c = C_1 + C_2$

C_1 is the covariance associated with population 1

C_2 is the covariance associated with population 2

$\boldsymbol{m}_1$ is the mean of population 1

$\boldsymbol{m}_2$ is the mean of population 2

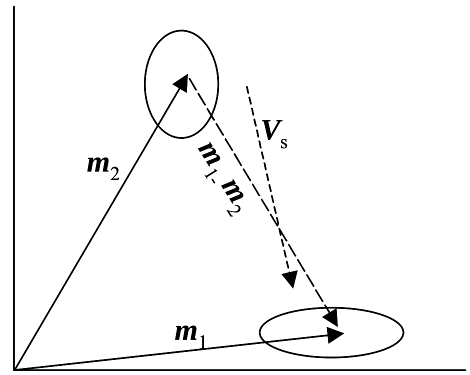

Figure 17. Non-isotropic Noise Case

The Fisher Linear Discriminant uses the inverse of the combined covariance matrix to rotate the vector between the population means to produce maximum statistical separation.

Our problem involves deriving the entries in a confusion matrix. For each row of the confusion matrix, the true target is presumed to be known. Therefore, we would have to modify the Fisher Linear Discriminant process slightly for our needs. Specifically, when evaluating a row of the confusion matrix, only one covariance matrix applies (the one for the presumed target). The means could then be the locations of the mean for the presumed target and the locations of the means for each of the other targets included in the confusion matrix. A number of such pair-wise decisions would essentially put a hyper-box around the presumed target and the probability of being within that hyper-box would define the diagonal term on the confusion matrix. The sides of the hyper-box would be defined by the separation vector, $\boldsymbol{V}_s$, but a constant would need to be set to define the location of each of these hyper planes. The constant could be defined so the plane passes through the midpoint of the line separating the target means. Alternatively, a no-declare buffer region could be established between each target pair to reduce the chances of false reports. The off-diagonal terms would be found by calculating the probability that the observed return for a target would be outside the hyper-box and closer to the other targets.

F. DISCRIMINATION AMONG TARGETS WITHIN A CLASS

One might wish to implement a two-stage process in which a target is first evaluated against a class (to take advantage of the potentially better orthogonality among class templates) and then determine the specific target type within a class. The prior section described the approach to the first stage, but a different process appears warranted for the second stage. The idea here is to remove as much of the common information from the individual vectors as possible and then test for differences among the resulting modified vectors. Figure 18 depicts this process. The left part of the figure shows the original arrangement of the target vectors that make up the target class, the composite vector used to represent the entire class, and the error ellipse due to sensor noise for one of the target vectors. The right part of the figure shows the resulting vectors after the composite vector has been subtracted from each of the individual vectors. The resulting modified vectors have clearly become more orthogonal. However, if the modified vectors are re-normalized, then the noise-error ellipse will become larger as also shown in the figure.

This process has made the problem of discrimination among the individual targets within a class amenable to the analysis procedures described above because of the near orthogonality of the modified vectors. Because of the renormalization of both the modified vectors and the size of the error ellipse, however, the analysis process may require substantially higher SNRs to distinguish individual targets within a class. The feasibility of this target-type discrimination will therefore depend upon the degree of difference among the vectors within a class and the signal-to-noise levels.

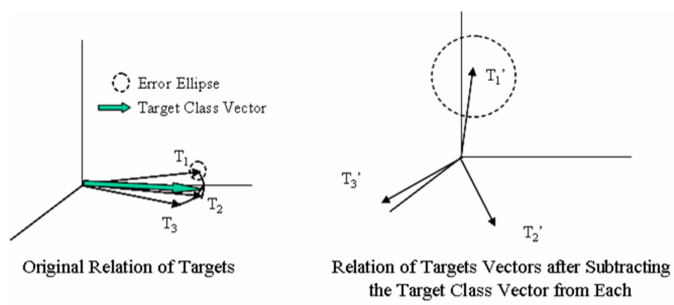

Figure 18. Effect of Removing the Target Class Vector

G. DEALING WITH A MIX OF HIGHLY CORRELATED AND NEARLY UNCORRELATED TARGETS

One might sometimes encounter a situation similar to the one depicted in Figure 19. In this case, two of the targets have nearly aligned template vectors (and are therefore highly correlated), but the third has a nearly orthogonal template vector (and is therefore nearly uncorrelated with the other two). The analysis procedure described in Section V generally assumes that the individual target vectors are uncorrelated, that is, $f(x, y, z) = f(x) \cdot f(y) \cdot f(z)$. In this case, which involves a mix of highly correlated and nearly uncorrelated targets, the joint probability distribution would only partly factor, such that

$f(x, y, z) = f(x, y) \cdot f(z)$. Therefore, in this case the general equation (3) could be rewritten as

$$\begin{aligned} P(X \mid T_i) &= P(x > y \text{ and } x > z) \\ &= \int_{-\infty}^{\infty} dx \int_{-\infty}^{x} f_{T_i}(x, y) F_{T_i}(x) dy \end{aligned} \tag{50}$$

because

$$\int_{-\infty}^{x} f_{T_i}(x, y) f_{T_i}(z) dz = f_{T_i}(x, y) F_{T_i}(x) \ . \tag{51}$$

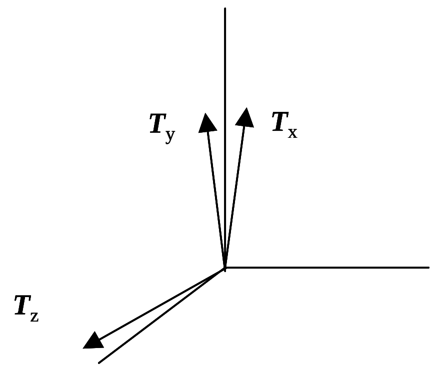

Following dot products apply:
$\boldsymbol{T}_{\mathrm{x}} \cdot \boldsymbol{T}_{\mathrm{y}} \approx 1$
$\boldsymbol{T}_{\mathrm{x}} \cdot \boldsymbol{T}_{\mathrm{z}} \approx 0$
$\boldsymbol{T}_{\mathrm{y}} \cdot \boldsymbol{T}_{\mathrm{z}} \approx 0$

Figure 19. Mix of Highly Correlated and Uncorrelated Targets

This procedure may prove useful if the majority of the targets are uncorrelated and only a few are highly correlated. The following provides a formulation for representing the joint density of two partially correlated Gaussian random variables:

$$f(x, y) = \frac{1}{2\pi\sigma_x\sigma_y\sqrt{1-r^2}} \exp\left(-\frac{1}{2(1-r^2)}\left[\frac{(x-m_x)^2}{\sigma_x^2} - \frac{2r(x-m_x)(y-m_y)}{\sigma_x\sigma_y} + \frac{(y-m_y)^2}{\sigma_y^2}\right]\right) \tag{52}$$

where m_x, σ_x, m_y, and σ_y are the mean and standard deviation of the random variables x and y and r is the correlation between the two random variables. This is actually the two-dimensional version of the multidimensional Gaussian, (25), given previously.

H. EFFECT OF DIMENSIONALITY OF TARGET TEMPLATE VECTORS

The dimensionality of the target vectors affects the ability to differentiate between targets for the noncoherent case for the reasons described below.[21] To address this issue, consider the simplest case of target vectors $\boldsymbol{S}_1 = (1\ 0)^T$ and $\boldsymbol{S}_2 = (a\ b)^T$.

---

[21] The goal here is to offer a simple demonstration of a potential problem rather than to provide a rigorous analysis involving the use of SNR-dependent target templates as discussed in Chapter V.C.

Making $|\boldsymbol{S}_2| = 1$ requires $a < 1$ and $b = \sqrt{1-a^2}$. The correlation between these vectors is $\boldsymbol{S}_1 \cdot \boldsymbol{S}_2 = a$, and the magnitude of their difference is $|\boldsymbol{S}_1 - \boldsymbol{S}_2| = \sqrt{2(1-a)}$. Assuming the noise value is $\varepsilon << 1$, the first component of the expected measurement vector of target 1, that is, $< \boldsymbol{Z}_1 >$, can be approximated by 1, and the second component is given by $\varepsilon = \sqrt{\frac{\pi}{2}}\sigma$ because there is no signal in this measurement bin and the mean of the Rayleigh distribution applies. Hence, $< \boldsymbol{Z}_1 > \approx (1\,\varepsilon)^T$. In this case $< \boldsymbol{Z}_1 >^T \boldsymbol{S}_1 = 1$ and $< \boldsymbol{Z}_1 >^T \boldsymbol{S}_2 = a + \varepsilon\sqrt{1-a^2}$ (noncoherent case), so the dot product between the latter two vectors is a function of the SNR. Also note that for coherent processing, $< \boldsymbol{Z}_1 > = (1\ 0)^T$, such that $< \boldsymbol{Z}_1 >^T \boldsymbol{S}_1 = 1$ and $< \boldsymbol{Z}_1 >^T \boldsymbol{S}_2 = a$ (coherent case).

Hence, the dot product between the expected measurement, $< \boldsymbol{Z}_1 >$, and the template $\boldsymbol{S}_2$ varies with SNR for the noncoherent case but is invariant with SNR for the coherent case.

Now to consider higher dimensions (i.e., n dimensions), assume the following vectors:

$$\boldsymbol{S}_1 = (1\ 0\ 0\ 0\ 0 \ldots 0)^T \text{ and } \boldsymbol{S}_2 = (a\ b\ b\ b\ b \ldots b)^T, \text{ where } b = \sqrt{(1-a^2)/(n-1)}. \tag{53}$$

As before, let $< \boldsymbol{Z}_1 >$ be the expected return when target $\boldsymbol{S}_1$ is present. This yields

$< \boldsymbol{Z}_1 > = (1\ 0\ 0\ 0\ 0 \ldots 0)^{\mathrm{T}}$ for coherent processing and

$< \boldsymbol{Z}_1 > = (1\ \varepsilon\ \varepsilon\ \varepsilon\ \varepsilon \ldots \varepsilon)^T$ for noncoherent processing.

For coherent processing the dimensionality does not matter if the degree of correlation between the templates remains fixed, since

$$< \boldsymbol{Z}_1 >^T \boldsymbol{S}_1 = 1 \text{ and } < \boldsymbol{Z}_1 >^T \boldsymbol{S}_2 = a \text{ (coherent case).} \tag{54}$$

However, for noncoherent processing, one obtains

$$< \boldsymbol{Z}_1 >^T \boldsymbol{S}_1 = 1 \text{ and } < \boldsymbol{Z}_1 >^T \boldsymbol{S}_2 = a + \varepsilon\sqrt{(1-a^2)(n-1)}. \tag{55}$$

Figure 20 shows plots of (55) when $a = 0.6$ and $\varepsilon = 0.1$. This value of ε corresponds to an SNR of $1/2\sigma^2 = 25\pi$. The upper line corresponds to the first dot product, which is invariant with the number of dimensions. The second line, which corresponds to noncoherent processing, increases as the number of dimensions increases. This means that the likelihood of incorrectly recognizing target $\boldsymbol{Z}_1$ as target $\boldsymbol{S}_2$ would increase as the number of dimensions increases.[22] Of course, the reason for increasing the number of dimensions in the target vectors would be to enhance the ability to discriminate between two targets. Figure 21 shows how much decorrelation between the targets would be required to keep the chances of confusing target $\boldsymbol{Z}_1$ with target $\boldsymbol{S}_2$ constant when performing noncoherent target processing. The lower correlation curve in Figure 21 begins at a correlation of 0.6 for a two-dimensional case and falls to 0.057 for a 40-dimensional case. However, this reduced template correlation would lead to reduced target confusion if one were to perform coherent processing. In fact, the dot product for the coherent case would follow the lowest curve in Figure 21 (i.e., $\boldsymbol{S}_1^T \boldsymbol{S}_2 = <\boldsymbol{Z}_1>^T \boldsymbol{S}_2$ in the coherent case). Of course, the relationships depicted in Figs. 20 and 21 would change for different SNR assumptions (i.e., different values of ε) and target vectors different from those assumed in (53), and the vectors in (53) no doubt represent a worse case. For example, consider the following noncoherent case:

$$\boldsymbol{S}_1 = (\ 1\ 0\ 1\ 0\ 1\ 0\ldots)^T \sqrt{2/n} \tag{56a}$$

$$\boldsymbol{S}_2 = (\ 0.6\ 0.8\ 0.6\ 0.8\ 0.6\ 0.8\ldots)^T \sqrt{2/n} \tag{56b}$$

$$<\boldsymbol{Z}_1> \approx (\ 1\ \varepsilon\ 1\ \varepsilon\ 1\ \varepsilon\ldots)^T \sqrt{2/n} \tag{56c}$$

where the number of components in each vector is assumed to be even. In this case, the correlation between the two templates is given by $\boldsymbol{S}_1{}^T\boldsymbol{S}_2 = 0.6$, and the test statistics become $<\boldsymbol{Z}_1>^T \boldsymbol{S}_1 = 1$ and $<\boldsymbol{Z}_1>^T \boldsymbol{S}_2 = 0.6 + 0.8\ \varepsilon$. Therefore, although in this case the chance of confusing a measurement of target 1 with target 2 does not depend on the dimensionality of the vectors, it still depends on the size of the noise terms.

Both the cases shown in the figures and the numerical example involving (56) demonstrate a fundamental difference between the coherent and noncoherent cases and a need for caution when considering noncoherent processing.

[22] The reason that the $\boldsymbol{Z}_1 \bullet \boldsymbol{S}_2$ curve exceeds one is that our methodology does not include normalization of the measured vector, $\boldsymbol{Z}_1$. Also, because we are evaluating the noncoherent case, we can drop the magnitude so, for instance, $|<\boldsymbol{Z}_1>\cdot\boldsymbol{S}_2| = <\boldsymbol{Z}_1>\cdot\boldsymbol{S}_2$.

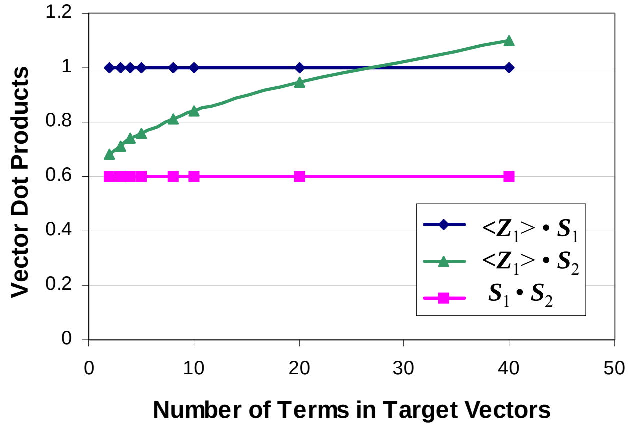

Figure 20. Effect of Dimensionality on Dot Products (Constant Correlation)

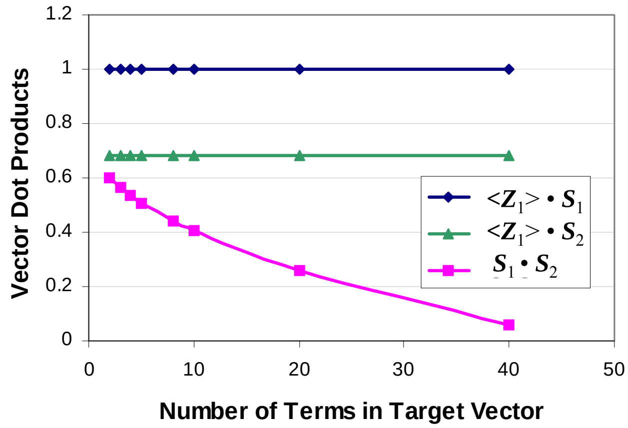

Figure 21. Effect of Variable Correlation on Vector Dot Products

VII. CONCLUSIONS

This paper provides a basis for the generation of confusion matrices. It demonstrates how to use target templates to derive traditional square confusion matrices that have identical row and column labels and how to generate rectangular matrices that typically include a no-declare, or no-decision, column. The paper suggests alternative criteria for generating the no-declare, or no-decision, column. The framework for generating confusion matrices presented herein could help ID system developers assess issues such as the following:

- What are the relative advantages of one-dimensional versus two-dimensional (or three-dimensional) target imaging?
- What are the relative benefits of higher versus lower resolution measurements (e.g., one-dimensional HRR profiles that use higher bandwidth to achieve more samples along the length of a target)?
- Because one-dimensional HRR profiles will vary depending upon the viewing angle of the target, what are the trade-offs involved in having separate templates for a few or a large number of different viewing angles? (For example, the target returns within a narrow set of viewing angles will likely be highly correlated, while those within a wider set of angles will begin to become uncorrelated, but will likely have greater variability due to scintillation effects.)
- How worthwhile is it to preserve phase information when generating target templates and making target measurements?

We address the first of these issues through a conventional approach of treating any target (template or measurement) as a vector of data points regardless of whether the process involves one-dimensional, two-dimensional, or higher diagonal target measurements. These vector representations provide a convenient way of understanding and evaluating the degree of correlation between targets, which has been shown to be directly related to the inner product of the vector representations for the various targets (assuming the vector representations have been normalized to one). Moreover, representation of one-, two- (or higher) dimensional targets as vectors leads to the calculation of the conditional probabilities appearing in the confusion matrices.

The paper considers coherent and noncoherent processing and correlated and uncorrelated targets. For the case of coherent processing of uncorrelated targets, the paper demonstrates the process for generating universal confusion matrices—that is, matrices that do not depend upon the details of the targets so long as the targets are uncorrelated. One winds up obtaining Rician random variables because of the need to compare the magnitudes of the test statistics (i.e., $R_{ik} = |T_{ik}|$). However, because the individual test statistics are uncorrelated, the required joint probability-distribution factors are easily obtained by multiplying the probability distributions associated with the individual test statistics. Although evaluation of cases involving uncorrelated targets and coherent processing is admittedly more of a theoretical than a practical case, this calculation provides insight into the upper limit of ID performance one can achieve as a function of the SNRs associated with measured targets.

We have illustrated the reduced likelihood of being able to identify targets as they become partially correlated. In fact, Figure 7 shows that there is very little error in analyzing targets as if they are uncorrelated if their actual correlation is less than 50 percent. To address partial target correlation, one requires the joint probability functions for partially correlated Rician random variables.

The paper demonstrates by means of simulation that the conditions under which the multidimensional Gaussian distribution adequately approximates the required joint probability function. In those cases where the Gaussian approximation would not hold, it would always be possible to construct the joint PDF using numerical techniques.

The paper also provides a methodology for performing noncoherent target processing. These latter cases, involving correlated targets and noncoherent processing, require application of the central limit theorem (i.e., normal approximations) to the Rician distribution. The correlated, noncoherent target cases reveal an interesting bias toward the declaration of targets that are closer to having a signature uniformly distributed over the measurement space as the SNR falls. This occurs if we simply apply our linear-statistic approach (16a) without modification when the SNR is low. However, if the templates for the noncoherent case are adjusted as a function of the SNR to reflect the expected return from a target, then this target-selection bias goes away. The paper further suggests how our process could be refined to deal with non-isotropic noise associated with either noncoherent processing or composite target templates corresponding to a target class. Also, we have shown that the noncoherent, correlated case can actually get worse as the number of elements in the measurement vector increases, unless the added dimensionality leads to a calculable reduction in the correlation between the targets.

Finally, the vector representation of target templates and measurements provides a useful way to think about the issues associated with making target class versus target type decisions.

APPENDIX—PROOFS

This appendix provides proofs of the mathematical claims made in the text. Throughout the appendix the superscript H is used to denote the Hermitian conjugate (complex conjugate transpose) of a complex vector or matrix.

A-1. Derivation of (8)

While (8) may be obvious, the following few equations further demonstrate why it is true. For the threshold condition $X_k \geq \alpha$, the probability of observing X_k, given true target t_i, is given by (5) with the lower limit on the final integral over x_k replaced by α:

$$P(X_k \,|\, T_i) = \int_{\alpha}^{\infty} f_{X_k}(x_k) dx_k \frac{\prod_{j=1}^{n} F_{X_j}(x_k)}{F_{X_k}(x_k)} . \tag{A1}$$

Next, examine the sum the sum of $P(X_k|t_i)$ over all target templates X_k:

$$\sum_{k=1}^{n} P(X_k \,|\, T_i) = \int_{\alpha}^{\infty} \prod_{j=1}^{n} F_{X_j}(x_k) \sum_{k=1}^{n} \frac{f_{X_k}(x_k)}{F_{X_k}(x_k)} dx_k . \tag{A2}$$

Now recognize that the integrand can be written as the derivative of the product of all cumulative functions, that is,

$$\frac{d}{dx_k} \prod_{j=1}^{n} F_{X_j}(x_k) = \prod_{j=1}^{n} F_{X_j}(x_k) \sum_{k=1}^{n} \frac{f_{X_k}(x_k)}{F_{X_k}(x_k)} . \tag{A3}$$

It follows that

$$\begin{aligned} \sum_{k=1}^{n} P(X_k \,|\, T_i) &= \int_{\alpha}^{\infty} d\left(\prod_{j=1}^{n} F_{X_j}(x_k) \right) \\ &= \prod_{j=1}^{n} F_{X_j}(\infty) - \prod_{j=1}^{n} F_{X_j}(\alpha) = 1 - \prod_{j=1}^{n} F_{X_j}(\alpha) \end{aligned} \tag{A4}$$

where we have used the fact that cumulative probability functions are unity at infinity. The sum over all states, including the no-declare state, must be unity, that is

$$\sum_{k=1}^{n} P(X_k \,|\, T_i) + P(ND \,|\, T_i) = 1 . \tag{A5}$$

From this and (A4) one arrives at (8) in the paper,

$$P(ND\,|\,T_i) = \prod_{j=1}^{n} F_{X_j}(\alpha)\,. \tag{A6}$$

Setting $\alpha = -\infty$ restores the no-threshold result $P(ND|t_i) = 0$, as required.

A-2. Vector Relations

In this section we derive several statistical results concerning template, noise, and signal vectors, and we point out results that are mentioned in the paper.

Let ***S*** be an *n*-dimensional, complex-valued template vector with norm 1:

$$S_\alpha = x_\alpha + iy_\alpha\ ,\ \alpha = 1,2,\cdots,n$$
$$|\boldsymbol{S}|^2 = \boldsymbol{S}^H\boldsymbol{S} = \sum_{\alpha=1}^{n}(x_\alpha^2 + y_\alpha^2) = 1\,.$$

Let ***N*** be an *n*-dimensional, complex-valued noise vector whose real and imaginary components are independent zero-mean Gaussian random processes with standard deviation σ:

$$N_\alpha = u_\alpha + iv_\alpha\ ,\ \alpha = 1,2,\cdots,n$$
$$<u_\alpha> = <v_\alpha> = 0$$
$$<u_\alpha u_\beta> = <v_\alpha v_\beta> = \sigma^2\delta_{\alpha\beta}$$
$$<u_\alpha v_\beta> = 0, \text{for all } \alpha \text{ and } \beta$$

Let ***Z*** be a complex-valued, *n*-dimensional signal vector given by $Z = S + N$.

Some useful relations follow.

a. $<|\boldsymbol{N}|^2> = <\boldsymbol{N}^H\boldsymbol{N}> = 2n\sigma^2$.

Proof:

$$<\boldsymbol{N}^H\boldsymbol{N}> = \sum_{\alpha=1}^{n}<N_\alpha^* N_\alpha> = \sum_{\alpha=1}^{n}<u_\alpha^2 + v_\alpha^2> = 2n\sigma^2\,.$$

b. Cov(***N***)=$<\boldsymbol{N}\boldsymbol{N}^H> = 2\sigma^2\boldsymbol{I}$, where ***I*** is the *n*-dimensional identity matrix. This is (12) in the paper.

Proof:

$$<N_a N_\beta^*> = <(u_a + iv_\alpha)(u_\beta - iv_\beta)> = <u_a u_\beta + v_\alpha v_\beta> = 2\sigma^2\delta_{\alpha\beta}\,.$$

c. $<|\boldsymbol{S}^H\boldsymbol{N}|^2> = 2\sigma^2$.

Proof:

$$<\left|\boldsymbol{S}^H N\right|^2> = <(S^H N)(S^H N)^*> = <\boldsymbol{S}^H NN^H S> = S^H <NN^H> S = 2\sigma^2 .$$

d. $<|\boldsymbol{Z}|^2> = 1 + 2n\sigma^2$.

Proof:

$$<|Z|^2> = <|S+N|^2> = <(S^H + N^H)(S+N)> = <S^H S + S^H N + N^H S + N^H N>$$

$$= 1 + \boldsymbol{S}^H <\boldsymbol{N}> + <\boldsymbol{N}^H> \boldsymbol{S} + <\boldsymbol{N}^H \boldsymbol{N}> = 1 + 2n\sigma^2 .$$

e. $<\boldsymbol{Z}\boldsymbol{Z}^H> = \boldsymbol{S}\boldsymbol{S}^H + 2\sigma^2 \boldsymbol{I}$.

Proof:

$$<\boldsymbol{Z}\boldsymbol{Z}^H> = <(\boldsymbol{S}+N)(\boldsymbol{S}+N)^H> = <\boldsymbol{S}\boldsymbol{S}^H + \boldsymbol{S}N^H + N^H\boldsymbol{S} + NN^H> = \boldsymbol{S}\boldsymbol{S}^H + 2\sigma^2 \boldsymbol{I} .$$

f. $<\left|\boldsymbol{S}^H \boldsymbol{Z}\right|^2> = 1 + 2\sigma^2$.

Proof:

$$<\left|\boldsymbol{S}^H \boldsymbol{Z}\right|^2> = <(\boldsymbol{S}^H \boldsymbol{Z})(\boldsymbol{S}^H \boldsymbol{Z})^H> = \boldsymbol{S}^H <\boldsymbol{Z}\boldsymbol{Z}^H> \boldsymbol{S} = 1 + 2\sigma^2 .$$

A-3. Rayleigh Probability Density Function

Here we show that the amplitude of the components of the noise vector $\boldsymbol{N}$ have a Rayleigh PDF. Consider a component of $\boldsymbol{N}$ given by $u + iv$. Since u and v are independent, zero-mean Gaussians, their joint PDF is given by the two-dimensional Gaussian:

$$\rho(u,v) = \tfrac{1}{2\pi\sigma^2} e^{-\frac{(u^2+v^2)}{2\sigma^2}} . \tag{A7}$$

Switching to polar coordinates and accounting for the Jacobian, one obtains an element of probability in terms of the joint PDF expressed in polar coordinates,

$$\rho_P(r,\theta) r dr d\theta = \tfrac{1}{2\pi\sigma^2} e^{-\frac{r^2}{2\sigma^2}} r dr d\theta . \tag{A8}$$

Integrating over all θ gives

$$\rho_{\mathrm{RAY}}(r) dr = \int_0^{2\pi} \rho_P(r,\theta) d\theta r dr = \tfrac{r}{\sigma^2} e^{-\frac{r^2}{2\sigma^2}} dr \tag{A9}$$

where we identify $\rho_{\mathrm{RAY}}(r)$ as the Rayleigh PDF. It is straightforward to show that $<r>=\sqrt{\frac{\pi}{2}}\sigma$ and $<r^2>=2\sigma^2$, from which the standard deviation is given by $\sqrt{<r^2>-<r>^2}=\sqrt{2-\frac{\pi}{2}}\sigma$.

A-4. Rician Probability Density Function

In this section we prove that the amplitude of each component of the signal vector ***Z*** has a Rician PDF. We also present some useful properties of the Rician PDF. Consider a component of ***Z*** = ***S*** + ***N***, given by $(x + iy)+(u + iv) = a + ib$. Similar to the above analysis, the joint PDF of a and b is given by

$$\rho(a,b)=\frac{1}{2\pi\sigma^2}e^{-\frac{(a-x)^2+(b-y)^2}{2\sigma^2}}. \quad \text{(A10)}$$

Letting $a = r\cos\theta$, $b = r\sin\theta$, $x = A\sin\phi$, $y = A\sin\phi$, an element of probability in polar coordinates (r,θ) becomes

$$\rho_P(r,\theta)rdrd\theta=\frac{1}{2\pi\sigma^2}e^{-\frac{(r^2+A^2-2rA\cos(\theta-\phi))}{2\sigma^2}}rdrd\theta. \quad \text{(A11)}$$

Integrating over all θ gives

$$\begin{aligned}\rho_{\mathrm{RIC}}(r)dr&=\int_0^{2\pi}\rho_P(r,\theta)d\theta rdr\\&=\frac{r}{2\pi\sigma^2}e^{-\frac{(r^2+A^2)}{2\sigma^2}}\int_0^{2\pi}e^{\frac{rA\cos(\theta-\phi)}{\sigma^2}}d\theta dr\end{aligned}. \quad \text{(A12)}$$

Since the θ integral is over all angles, it is independent of the angle ϕ and is given by [9]

$$\int_0^{2\pi}e^{\frac{rA\cos(\theta-\phi)}{\sigma^2}}d\theta=2\pi I_0(\frac{rA}{\sigma^2}) \quad \text{(A13)}$$

where I_0 is the zeroth-order modified Bessel function of the first kind. Finally, the Rician PDF is given by

$$\rho_{\mathrm{RIC}}(r)=\frac{r}{\sigma^2}e^{-\frac{(r^2+A^2)}{2\sigma^2}}I_0(\frac{rA}{\sigma^2}). \quad \text{(A14)}$$

Note that for $A = 0$, the Rician density reduces to the Rayleigh density appearing in (A9).

The mean value of the Rician is found from Mathematica to be

$$<r>=\frac{\sigma}{2}\sqrt{\frac{\pi}{2}}e^{-\frac{A^2}{4\sigma^2}}\left((2+\frac{A^2}{\sigma^2})I_0(\frac{A^2}{4\sigma^2})+\frac{A^2}{\sigma^2}I_1(\frac{A^2}{4\sigma^2})\right) \quad \text{(A15)}$$

where I_1 is the first-order modified Bessel function of the first kind. The mean can also be expressed in terms of a confluent hypergeometric function [10]. The Bessel function representation lends itself to obtaining expressions for the mean value for large and for small values of A for high and low SNR. When $A/\sigma > 1$ the modified Bessel functions can be approximated by their asymptotic expansions for large arguments [5]:

$$I_0(x) \sim \tfrac{1}{\sqrt{2\pi x}} e^x (1 + \tfrac{1}{8x} + \cdots) \,. \tag{A16a}$$

$$I_1(x) \sim \tfrac{1}{\sqrt{2\pi x}} e^x (1 - \tfrac{3}{8x} + \cdots) \,. \tag{A16b}$$

Using these expressions in (A15), one finds an expression for the mean of a Rician for high signal to noise to order $(\sigma/A)^2$:

$$< r > \approx A(1 + \tfrac{\sigma^2}{2A^2}) \,. \tag{A17}$$

For low signal to noise ($A/\sigma<1$), the Bessel functions can be expanded around zero [9]:

$$I_0(x) = 1 + \frac{x^2}{4} + \cdots \tag{A18a}$$

$$I_1(x) = \frac{x}{2} + \frac{x^3}{16} + \cdots \tag{A18b}$$

After expanding the exponential in (A15), substituting the approximations (A18) into (A15), and retaining terms to order A^2/σ^2, one finds

$$< r > \approx \sigma \sqrt{\tfrac{\pi}{2}} \left(1 + \tfrac{A^2}{4\sigma^2} \right). \tag{A19}$$

The second moment of the Rician is computed easily from the definition of r^2:

$$< r^2 > = < a^2 + b^2 > = < (x+u)^2 + (y+v)^2 > = < A^2 + 2(xu + yv) + u^2 + v^2 > \tag{A20}$$

where the averages are performed over the Gaussians u and v. Only the even terms in u and v survive, giving

$$< r^2 > = A^2 + 2\sigma^2 \,. \tag{A21}$$

If the parameter A has been normalized to one, then $< r^2 > = 1 + 2\sigma^2$, as appears in (19) in the text. The variance of the Rician is given by

$$\sigma^2_{\mathrm{RIC}} = < r^2 > - < r >^2 \,. \tag{A22}$$

For high signal to noise the variance, through (A22), (A21), and (A17), becomes

$$\sigma^2_{\mathrm{RIC}} \approx \sigma^2 (1 - \tfrac{\sigma^2}{4A^2}) \tag{A23}$$

valid to order $(\sigma/A)^2$.

Finally, it is useful to find conditions under which the Rician PDF can be approximated by a Gaussian PDF. Starting with the Rician PDF in (A14) and using the asymptotic expansion of I_0 for large arguments (A16a), one has to leading order

$$\rho_{\mathrm{RIC}}(r) \sim \sqrt{\tfrac{r}{A}}\left(\frac{1}{\sqrt{2\pi}\sigma} e^{-\frac{(r-A)^2}{2\sigma^2}}\right). \tag{A24}$$

The term in parentheses is recognized as a Gaussian with mean A and standard deviation σ. When σ is sufficiently small, the density is appreciable only near $r = A$; in this event, the prefactor $\sqrt{r/A}$ is of order unity, and the density is approximately Gaussian. Recapping, the conditions for the Rician PDF to be approximated by a Gaussian are $\sigma/A \ll 1$ and $r \sim A$.

A-5. Coherent Processing Results

In this section we derive the main coherent processing results mentioned in the text. We start with the covariance matrix result stated near the conclusion of Section IV [after (17)]. For each true target $\boldsymbol{S}_i$, form the signal vector $\boldsymbol{Z}_i = \boldsymbol{S}_i + \boldsymbol{N}$ and the n complex random variables $T_{ik} = \boldsymbol{S}_k^H \boldsymbol{Z}_i$ $k = 1, 2, \ldots, n$. The covariance matrix is given by

$$C_{jk} = \left\langle (T_{ij} - < T_{ij} >)^* (T_{ik} - < T_{ik} >) \right\rangle . \tag{A25}$$

Now, $< T_{ik} > = < \boldsymbol{S}_k^H \boldsymbol{Z}_i > = < \boldsymbol{S}_k^H \boldsymbol{S}_i + \boldsymbol{S}_k^H \boldsymbol{N} > = \boldsymbol{S}_k^H \boldsymbol{S}_i$, and similarly $< T_{ij} > = \boldsymbol{S}_j^H \boldsymbol{S}_i$. Therefore,

$$C_{jk} = \left\langle (\boldsymbol{S}_j^H \boldsymbol{N})^* (\boldsymbol{S}_k^H \boldsymbol{N}) \right\rangle = \boldsymbol{S}_k^H < \boldsymbol{N}\boldsymbol{N}^H > \boldsymbol{S}_j = 2\sigma^2 \boldsymbol{S}_k^H \boldsymbol{S}_j \tag{A26}$$

where the last equality follows from relation A-2b above. Note that the covariance matrix is independent of the true target $\boldsymbol{S}_i$. If the targets $\boldsymbol{S}_k$ and $\boldsymbol{S}_j$ are orthogonal, then $C_{jk} = 2\sigma^2 \delta_{jk}$ [(18) in the text].

It is shown below that when the signal and template vectors are matched, the amplitude $R_{ii} = |T_{ii}|$ is a Rician random variable with parameters $A = 1$ and σ. Then, from (A21) $< R_{ii}^2 > = 1 + 2\sigma^2$. If the targets $\boldsymbol{S}_k$ and $\boldsymbol{S}_i$ are independent, then the amplitudes R_{ik} and R_{ij} are independent with joint expectation given by

$$< R_{ij} R_{ik} > = (1 + 2\sigma^2)\delta_{jk} . \tag{A27}$$

This is (19) in the text.

We now show that, in general, the amplitudes $R_{ik} = |T_{ik}|$ are Rician random variables. Decomposing T_{ik} into real and imaginary parts, $T_{ik} = P + iQ$, one finds

$$P = \mathrm{Re}\left(\boldsymbol{S}_k^H \boldsymbol{Z}_i\right) = \mathrm{Re}\left(\boldsymbol{S}_k^H (\boldsymbol{S}_i + \boldsymbol{N})\right)$$

$$= \mathrm{Re}(\boldsymbol{S}_k^H \boldsymbol{S}_i) + \mathrm{Re}\left(\sum_{a=1}^{n} (X_\alpha - iY_\alpha)(u_\alpha + iv_\alpha)\right)$$

$$= \mathrm{Re}(\boldsymbol{S}_k^H \boldsymbol{S}_i) + \sum_{a=1}^{n} (X_\alpha u_\alpha + Y_\alpha v_\alpha)\ . \tag{A28}$$

Similarly,

$$Q = \mathrm{Im}\left(\boldsymbol{S}_k^H \boldsymbol{Z}_i\right) = \mathrm{Im}(\boldsymbol{S}_k^H \boldsymbol{S}_i) + \sum_{\alpha=1}^{n} (X_\alpha v_\alpha - Y_\alpha u_\alpha)\ . \tag{A29}$$

P and Q are then real Gaussian random variables; their means and variances follow. Thus, $< P >= \mathrm{Re}\left(\boldsymbol{S}_k^H \boldsymbol{Z}_i\right)$ and $< Q >= \mathrm{Im}\left(\boldsymbol{S}_k^H \boldsymbol{Z}_i\right)$. Then

$$\sigma_P^2 =< (P- < P >)^2 >= \left\langle \left(\sum_{\alpha=1}^{n} X_\alpha u_\alpha + Y_\alpha v_\alpha \right)^2 \right\rangle = \left\langle \sum_{\alpha,\beta=1}^{n} (X_\alpha u_\alpha + Y_\alpha v_\alpha)(X_\beta u_\beta + Y_\beta v_\beta) \right\rangle$$

$$= \sum_{a,\beta=1}^{n} \begin{matrix} X_\alpha X_\beta < u_\alpha u_\beta > + X_\alpha Y_\beta < u_\alpha v_\beta > \\ + Y_\alpha X_\beta < v_\alpha u_\beta > + Y_\alpha Y_\beta < v_\alpha v_\beta > \end{matrix}$$

$$= \sigma^2 \sum_{a=1}^{n} ({X_\alpha}^2 + {Y_\alpha}^2) = \sigma^2 \tag{A30}$$

where the final result follows from the normalization of $\boldsymbol{S}_k$. A similar calculation yields

$$\sigma_Q^2 =< (Q- < Q >)^2 >= \sigma^2\ . \tag{A31}$$

It is also straightforward to verify that $\sigma_{PQ}^2 =< (P- < P >)(Q- < Q >) >= 0$, from which it follows that P and Q are *independent* Gaussian random variables. Hence, the joint distribution of P and Q is

$$\rho_J(P,Q) = \frac{1}{2\pi\sigma^2} e^{-\frac{(P-\mathrm{Re}(\boldsymbol{S}_k^H \boldsymbol{S}_i))^2 + (Q-\mathrm{Im}(\boldsymbol{S}_k^H \boldsymbol{S}_i))^2}{2\sigma^2}} \tag{A32}$$

which is identical in form to (A10). We conclude that $R_{ik} = |T_{ik}| = \sqrt{P^2 + Q^2}$ has the Rician PDF

$$f_{ik}(R_{ik}) = \tfrac{R_{ik}}{\sigma^2} e^{-\frac{({R_{ik}}^2 + {c_{ik}}^2)}{2\sigma^2}} I_0(\tfrac{R_{ik} c_{ik}}{\sigma^2}) \tag{A33}$$

where $c_{ik} = |\boldsymbol{S}_k^H \boldsymbol{S}_i|$. This is (24) in the text. For $i = k$ (perfect overlap), $c_{ik} = 1$, whereas for independent targets, $c_{ik} = 0$, and the Rician reduces to a Rayleigh PDF (21)

For correlated targets, the joint expectation $<R_{ij}R_{ik}>$ cannot be computed exactly; however, an approximate relation can be found to order σ^2, as outlined in the following.

$$<R_{ij}R_{ik}>=<|\boldsymbol{S}_j^H\boldsymbol{Z}_i||\boldsymbol{S}_k^H\boldsymbol{Z}_i|>=<|\boldsymbol{S}_j^H\boldsymbol{Z}_i\boldsymbol{Z}_i^H\boldsymbol{S}_k|>=<|\boldsymbol{S}_j^H(\boldsymbol{S}_i+\boldsymbol{N})(\boldsymbol{S}_i+\boldsymbol{N})^H\boldsymbol{S}_k|>$$

$$=<|\boldsymbol{S}_j^H\boldsymbol{S}_i\boldsymbol{S}_i^H\boldsymbol{S}_k+\boldsymbol{S}_j^H\boldsymbol{S}_i\boldsymbol{N}^H\boldsymbol{S}_k+\boldsymbol{S}_j^H\boldsymbol{N}\boldsymbol{S}_i^H\boldsymbol{S}_k+\boldsymbol{S}_j^H\boldsymbol{N}\boldsymbol{N}^H\boldsymbol{S}_k|> \tag{A34}$$

Defining $D=\boldsymbol{S}_j^H\boldsymbol{S}_i\boldsymbol{S}_i^H\boldsymbol{S}_k$, $E=\boldsymbol{S}_j^H\boldsymbol{S}_i\boldsymbol{N}^H\boldsymbol{S}_k$, $F=\boldsymbol{S}_j^H\boldsymbol{N}\boldsymbol{S}_i^H\boldsymbol{S}_k$, and $G=\boldsymbol{S}_j^H\boldsymbol{N}\boldsymbol{N}^H\boldsymbol{S}_k$, the joint expectation becomes

$$\begin{aligned}<R_{ij}R_{ik}>&=<\sqrt{(D+E+F+G)(D+E+F+G)^*}>\\&=<\{|D|^2+|E|^2+|F|^2+|G|^2+DE^*+DF^*+DG^*+ED^*\\&+EF^*+EG^*+FD^*+FE^*+FG^*+GD^*+GE^*+GF^*\}^{\frac{1}{2}}>\end{aligned} \tag{A35}$$

In anticipation of expanding the square root, we retain terms up to quadratic order in the noise vector,

$$<R_{ij}R_{ik}>\approx<(|D|^2+K+L)^{\frac{1}{2}}> \tag{A36}$$

where K contains the first-order terms in $\boldsymbol{N}$ and L contains second-order terms in $\boldsymbol{N}$, with

$$K=DE^*+ED^*+DF^*+FD^* \tag{A37a}$$

$$L=|E|^2+|F|^2+DG^*+GD^*+EF^*+FE^*. \tag{A37b}$$

Expanding the square root, the joint expectation becomes

$$<R_{ij}R_{ik}>\approx|D|<\{1+\tfrac{1}{2|D|^2}(K+L)-\tfrac{1}{8|D|^4}(K+L)^2\}>. \tag{A38}$$

Since K is linear in $\boldsymbol{N}$, the average over K vanishes. Again, keeping terms up to quadratic order (A38) becomes

$$<R_{ij}R_{ik}>\approx|D|(1+\tfrac{<L>}{2|D|^2}-\tfrac{<K^2>}{8|D|^4}). \tag{A39}$$

Before computing the averages $<L>$ and $<K^2>$, it is beneficial to examine which terms survive the averaging process. Consider the term FE^* in $<L>$,

$$<FE^*>=<(\boldsymbol{S}_j^H\boldsymbol{N}\boldsymbol{S}_i^H\boldsymbol{S}_k)(\boldsymbol{S}_j^H\boldsymbol{S}_i\boldsymbol{N}^H\boldsymbol{S}_k)^*>=<\boldsymbol{S}_j^H\boldsymbol{N}\boldsymbol{S}_k^H\boldsymbol{N}>\boldsymbol{S}_i^H\boldsymbol{S}_k\boldsymbol{S}_j^H\boldsymbol{S}_i. \tag{A40}$$

Let the noise vector be denoted by $\boldsymbol{N}=(\eta_1,\eta_2,\cdots,\eta_n)^T$. Now, the average in (A40) is an average over a quadratic form in the components of N,

$$<\boldsymbol{S}_j^H\boldsymbol{N}\boldsymbol{S}_k^H\boldsymbol{N}>=\sum_{\alpha,\beta=1}^{n}C_{\alpha\beta}<\eta_\alpha\eta_\beta> \tag{A41}$$

where the coefficients $C_{\alpha\beta}$ depend on the template vectors $\boldsymbol{S}_j$ and $\boldsymbol{S}_k$. Since the components of $\boldsymbol{N}$ are independent and $<\eta_\alpha>=0$, the only terms that could potentially be nonzero are the "diagonal" terms $<\eta_\alpha^2>$; however, writing $\eta_\alpha = u_\alpha + iv_\alpha$ one has

$$<\eta_\alpha^2> = <u_\alpha^2 - v_\alpha^2 + 2iu_\alpha v_\alpha> = 0 \tag{A42}$$

and the average $<FE*>$ vanishes. We conclude that *all averages containing quadratic forms in* $\boldsymbol{N}$ or $\boldsymbol{N}^H$ *vanish*; *only those average that contain both* $\boldsymbol{N}$ *and* $\boldsymbol{N}^H$ *survive*. For the average over $<L>$ the surviving terms are $<|E|^2>$, $<|F|^2>$, $<DG^*>$, and $<GD^*>$, which we now compute:

$$<|E|^2> = <(\boldsymbol{S}_j^H\boldsymbol{S}_i\boldsymbol{N}^H\boldsymbol{S}_k)(\boldsymbol{S}_j^H\boldsymbol{S}_i\boldsymbol{N}^H\boldsymbol{S}_k)^*> = \boldsymbol{S}_j^H\boldsymbol{S}_i\boldsymbol{S}_k^H <\boldsymbol{N}\boldsymbol{N}^H> \boldsymbol{S}_k\boldsymbol{S}_i^H\boldsymbol{S}_j$$

$$= 2\sigma^2\left|\boldsymbol{S}_j^H\boldsymbol{S}_i\right|^2, \text{ since } \boldsymbol{S}_k^H <\boldsymbol{N}\boldsymbol{N}^H> \boldsymbol{S}_k = 2\sigma^2\boldsymbol{S}_k^H\boldsymbol{S}_k = 2\sigma^2. \tag{A43a}$$

$$<|F|^2> = <(\boldsymbol{S}_j^H\boldsymbol{N}\boldsymbol{S}_i^H\boldsymbol{S}_k)(\boldsymbol{S}_j^H\boldsymbol{N}\boldsymbol{S}_i^H\boldsymbol{S}_k)^*> = \boldsymbol{S}_j^H <\boldsymbol{N}\boldsymbol{N}^H> \boldsymbol{S}_j\boldsymbol{S}_i^H\boldsymbol{S}_k\boldsymbol{S}_k^H\boldsymbol{S}_i$$

$$= 2\sigma^2\left|\boldsymbol{S}_k^H\boldsymbol{S}_i\right|^2, \text{ since } \boldsymbol{S}_j^H <\boldsymbol{N}\boldsymbol{N}^H> \boldsymbol{S}_j = 2\sigma^2\boldsymbol{S}_j^H\boldsymbol{S}_j = 2\sigma^2. \tag{A43b}$$

$$<DG^*> = <(\boldsymbol{S}_j^H\boldsymbol{S}_i\boldsymbol{S}_i^H\boldsymbol{S}_k)(\boldsymbol{S}_j^H\boldsymbol{N}\boldsymbol{N}^H\boldsymbol{S}_k)^*> = \boldsymbol{S}_j^H\boldsymbol{S}_i\boldsymbol{S}_i^H\boldsymbol{S}_k\boldsymbol{S}_k^H <\boldsymbol{N}\boldsymbol{N}^H> \boldsymbol{S}_j$$

$$= 2\sigma^2(\boldsymbol{S}_j^H\boldsymbol{S}_i)(\boldsymbol{S}_k^H\boldsymbol{S}_i)^*(\boldsymbol{S}_j^H\boldsymbol{S}_k)^*, \text{ since } <\boldsymbol{N}\boldsymbol{N}^H> = 2\sigma^2\boldsymbol{I}. \tag{A43c}$$

$$<GD^*> = [<DG^*>]^* = 2\sigma^2(\boldsymbol{S}_j^H\boldsymbol{S}_i)^*(\boldsymbol{S}_k^H\boldsymbol{S}_i)(\boldsymbol{S}_j^H\boldsymbol{S}_k). \tag{A43d}$$

Letting $\boldsymbol{S}_j^H\boldsymbol{S}_i = c_{ij}e^{i\phi_{ij}}$, $\boldsymbol{S}_k^H\boldsymbol{S}_i = c_{ik}e^{i\phi_{ik}}$, and $\boldsymbol{S}_j^H\boldsymbol{S}_k = c_{kj}e^{i\phi_{kj}}$, such that, for example,

$$<|E|^2> = 2\sigma^2|\boldsymbol{S}_j^H\boldsymbol{S}_i|^2 = 2\sigma^2(\boldsymbol{S}_j^H\boldsymbol{S}_i)^*(\boldsymbol{S}_j^H\boldsymbol{S}_i) = 2\sigma^2 c_{ij}e^{-i\phi_{ij}}c_{ij}e^{i\phi_{ij}} = 2\sigma^2 c_{ij}^2$$

$$<DG^*> = 2\sigma^2 c_{ij}e^{i\phi_{ij}}c_{ik}e^{-i\phi_{ik}}c_{kj}e^{-i\phi_{kj}} = 2\sigma^2 c_{ij}c_{ik}c_{kj}e^{i(\phi_{ij}-\phi_{ik}-\phi_{kj})}$$

$<L>$ becomes $<L> = <|E|^2> + <|F|^2> + <DG^*> + <GD^*>$

$$= 2\sigma^2(c_{ij}^2 + c_{ik}^2 + 2c_{ij}c_{ik}c_{kj}\cos(\phi_{ij}-\phi_{ik}-\phi_{kj})). \tag{A44}$$

The surviving terms[23] of $<K^2>$ are

---

[23] We start with the following

$$\begin{aligned}<K^2> &= <(DE^* + ED^* + DF^* + FD^*)^2> = <(DE^*)^2> + <(ED^*)^2> + <(DF^*)^2> \\ &+ <(FD^*)^2> + 2<DE^*ED^*> + 2<DE^*DF^*> + 2<DE^*FD^*> + 2<ED^*DF^*> \\ &+ 2<ED^*FD^*> + 2<DF^*FD^*>\end{aligned}$$

and examine some of the terms to demonstrate which terms survive. For example:

$$<(DE^*)^2> = \left(\boldsymbol{S}_j^H\boldsymbol{S}_i\right)^2\left(\boldsymbol{S}_i^H\boldsymbol{S}_k\right)^2\left(\boldsymbol{S}_i^H\boldsymbol{S}_j\right)^2 <(\boldsymbol{S}_k^H\boldsymbol{N})^2> = \left(\boldsymbol{S}_j^H\boldsymbol{S}_i\right)^2\left(\boldsymbol{S}_i^H\boldsymbol{S}_k\right)^2\left(\boldsymbol{S}_i^H\boldsymbol{S}_j\right)^2 <\boldsymbol{S}_k^H\boldsymbol{N}\boldsymbol{S}_k^H\boldsymbol{N}>$$

but the term $<\boldsymbol{S}_k^H\boldsymbol{N}\boldsymbol{S}_k^H\boldsymbol{N}>$ is similar in form to (A41) and therefore equals zero. A similar argument applies to the other squared terms. Since D, E, and F are complex scalars, their order can be

$$< K^2 > = 2 < DE^* DF^* > +2 <| D |^2 | E |^2 > +2 <| D |^2 | F |^2 > +2 < ED^* FD^* > . \tag{A45}$$

Similar calculations to those involving $< L >$ yield

$$< K^2 > = 4\sigma^2 c_{ij} c_{ik} (c_{ij}^2 + c_{ik}^2 + 2c_{ij} c_{ik} c_{kj} \cos(\phi_{ij} - \phi_{ik} - \phi_{kj})) . \tag{A46}$$

Noting that $|D| = \left|\boldsymbol{S}_j^H \boldsymbol{S}_i\right| \left|\boldsymbol{S}_i^H \boldsymbol{S}_k\right| = c_{ij} c_{ik}$, substituting (A46) and (A44) into (A39) and simplifying, one finally gets

$$< R_{ij} R_{ik} > \approx c_{ij} c_{ik} + \frac{\sigma^2}{2c_{ij} c_{ik}} \left(c_{ij}^2 + c_{ik}^2 + 2c_{ij} c_{ik} c_{kj} \cos(\phi_{ij} - \phi_{ik} - \phi_{kj}) \right) \tag{A47}$$

valid to order σ^2 (actually to order σ^3, since the cubic terms vanish). This is (29) in the text.

A-6. Noncoherent Processing Results

In this section, we derive the covariance matrix result for the true target $\boldsymbol{A}_i$ [(39) in the text]. First, from the definition of the signal vector

$$\boldsymbol{Y}_i = (y_{i1}, y_{i2}, ..., y_{im})^T = | s_{i1} + n_1 |, | s_{i2} + n_2 |, ..., | s_{im} + n_m |)^T \tag{A48}$$

and it is clear from the discussions in Section A-4 that each component of $\boldsymbol{Y}_i$ is a Rician random variable with PDF

$$f_{ik}(y_{ik}) = \frac{y_{ik}}{\sigma^2} e^{-\frac{(y_{ik}^2 + a_{ik}^2)}{2\sigma^2}} I_0\left(\frac{y_{ik} a_{ik}}{\sigma^2}\right) . \tag{A49}$$

For each target vector $\boldsymbol{Y}_i$, associated with true target $\boldsymbol{A}_i$ but compared against target template $\boldsymbol{A}_k$, the test variables w_{ik} are given by

$$w_{ik} = \boldsymbol{A}_k{}^T \boldsymbol{Y}_i = \sum_{\alpha=1}^{m} a_{k\alpha} y_{i\alpha} , \; k = 1, 2, \ldots, n. \tag{A50}$$

The covariance matrix elements are given by

$$\begin{aligned} Q_{jk}(i) &\equiv <(w_{ij} - < w_{ij} >)(w_{ik} - < w_{ik} >)> \\ &= < w_{ij} w_{ik} > - < w_{ij} >< w_{ik} > . \end{aligned} \tag{A51}$$

---

interchanged such that $< DE^* ED^* > = < DD^* E^* E > = | D |^2 <| E |^2 >$. Also, $< DE^* FD^* > = | D |^2 < FE^* > = 0$, which follows (A41) and (A42). Finally, $< ED^* DF^* > = | D |^2 < EF^* > = 0$, which follows from (A41) with $\boldsymbol{N}$ replaced by $\boldsymbol{N}^{\mathrm{H}}$ or by recognizing that $< ED^* DF^* > [< DE^* FD^* >]^*$.

Then

$$
\begin{aligned}
Q_{jk}(i) &= <\boldsymbol{A}_j{}^T \boldsymbol{Y}_i \boldsymbol{A}_k{}^T \boldsymbol{Y}_i> - <\boldsymbol{A}_j{}^T \boldsymbol{Y}_i><\boldsymbol{A}_k{}^T \boldsymbol{Y}_i> \\
&= \boldsymbol{A}_j{}^T <\boldsymbol{Y}_i \boldsymbol{Y}_i^T> \boldsymbol{A}_k - \boldsymbol{A}_j{}^T <\boldsymbol{Y}_i><\boldsymbol{Y}_i^T> \boldsymbol{A}_k \\
&= \boldsymbol{A}_j{}^T (<\boldsymbol{Y}_i \boldsymbol{Y}_i^T> - <\boldsymbol{Y}_i><\boldsymbol{Y}_i^T>) \boldsymbol{A}_k \\
&= \boldsymbol{A}_j{}^T \mathrm{Cov}(\boldsymbol{Y}_i) \boldsymbol{A}_k
\end{aligned} \tag{A52}
$$

where $\mathrm{Cov}(\boldsymbol{Y}_i)$ is the covariance matrix for the signal vector $\boldsymbol{Y}_i$. Since the components of $\boldsymbol{Y}_i$ are independent Rician random variables, the covariance is diagonal with Rician variances on the diagonal,

$$\mathrm{Cov}(\boldsymbol{Y}_i)_{\alpha\beta} = \sigma_{i\alpha}^2 \delta_{\alpha\beta} \tag{A53}$$

with

$$\sigma_{i\alpha}^2 = <y_{i\alpha}^2> - <y_{i\alpha}>^2 \tag{A54}$$

where the mean and second moment of the Rician random variable $y_{i\alpha}$ are given in (A15) and (A21), respectively.

Substituting (A54) into (A53) yields

$$Q_{jk}(i) = \sum_{\alpha,\beta=1}^{n} a_{j\alpha} \sigma_{i\alpha}^2 \delta_{\alpha\beta} a_{k\beta} = \sum_{\alpha=1}^{m} a_{j\alpha} \sigma_{i\alpha}^2 a_{k\alpha} \tag{A55}$$

which is (39) in the text.

References

1. R. A. Mitchell and J. J. Westerkamp, “Robust statistical feature based aircraft identification,” *IEEE Trans. on Aerospace and Electronic Systems*, Vol. 35, No. 3, July 1999, pp. 1,077–1,094.

2. R. J Sullivan, *Radar Foundations for Imaging and Advanced Concepts*, Raleigh, NC: SciTech Publications, 2004.

3. J. K Haspert, “Optimum ID sensor fusion for multiple target types,” IDA Document D-2451, March 2000.

4. L. E. Brennan and I. S. Reed, “Theory of adaptive radar,” *IEEE Trans. Aerospace and Electronic Systems*, Vol. AES-9, No. 2, March 1973, pp. 237-252.

5. A. Dalcher, private communication. The integral (22c) is found in 6.633, #4 of I. S. Gradshteyn and I.M. Ryzhik, *Table of Integrals, Series, and Products, Corrected and Enlarged Edition,* Orlando: Academic Press, 1980.

6. P. Y. Kam, "Tight bounds on Rician-type error probabilities and some applications," *IEEE Trans. on Communications*, Vol. 42, No. 12, December 1994, pp. 3119–3128.

7. K. S. Miller, *Multidimensional Gaussian Distributions*, New York: Wiley, 1964.

8. R. O. Duda, Hart, P. E. and Stork, D. G., *Pattern Classification*, 2nd Ed., New York: Wiley, 2001.

9. R. S. Burlington and D. C. May, *Handbook of Probability and Statistics with Tables,* Sandusky, OH: Handbook Publishers, Inc., 1958.

10. J. Sijbers, A. J. den Dekker, P. Scheunders, and D. Van Dyck, "Maximum-likelihood estimation of Rician distribution parameters," *IEEE Transactions on Medical Imaging,* Vol. 17, No. 3, June 1998, pp. 357–361.

REPORT DOCUMENTATION PAGE						*Form Approved* *OMB No. 0704-0188*
Public reporting burden for this collection of information is estimated to average 1 hour per response, including the time for reviewing instructions, searching existing data sources, gathering and maintaining the data needed, and completing and reviewing this collection of information. Send comments regarding this burden estimate or any other aspect of this collection of information, including suggestions for reducing this burden to Department of Defense, Washington Headquarters Services, Directorate for Information Operations and Reports (0704-0188), 1215 Jefferson Davis Highway, Suite 1204, Arlington, VA 22202-4302. Respondents should be aware that notwithstanding any other provision of law, no person shall be subject to any penalty for failing to comply with a collection of information if it does not display a currently valid OMB control number. **PLEASE DO NOT RETURN YOUR FORM TO THE ABOVE ADDRESS.**						
1. REPORT DATE March 2005		2. REPORT TYPE Final				3. DATES COVERED *(From–To)* May 2003–June 2004
4. TITLE AND SUBTITLE General Approach to Template-Based Target Recognition						5a. CONTRACT NUMBER DASW01 04 C 0003
						5b. GRANT NUMBER
						5c. PROGRAM ELEMENT NUMBER
6. AUTHOR(S) J. Kent Haspert, James F. Heagy, Roger J. Sullivan						5d. PROJECT NUMBER
						5e. TASK NUMBER IDA Central Research Project C2081
						5f. WORK UNIT NUMBER
7. PERFORMING ORGANIZATION NAME(S) AND ADDRESS(ES) Institute for Defense Analyses 4850 Mark Center Drive Alexandria, VA 22311-1882						8. PERFORMING ORGANIZATION REPORT NUMBER IDA Paper NS P-3981
9. SPONSORING / MONITORING AGENCY NAME(S) AND ADDRESS(ES) Institute for Defense Analyses 4850 Mark Center Drive Alexandria, VA 22311-188						10. SPONSOR/MONITOR'S ACRONYM(S)
						11. SPONSOR/MONITOR'S REPORT NUMBER(S)
12. DISTRIBUTION / AVAILABILITY STATEMENT Approved for public release; distribution unlimited.						
13. SUPPLEMENTARY NOTES						
14. ABSTRACT The reported work began as an effort to understand the fundamental differences between target identification techniques based on one-dimensional high range resolution radar and two-dimensional range-Doppler-imaging radar. The work evolved into a more general statistical methodology using target templates to compute the entries in probability (or confusion) matrices, typically used to characterize combat identification (CID) systems. Starting with a set of complex-valued vector target templates, we present a systematic framework for generating and comparing a set of scalar test statistics and estimating their probability of occurrence. These probabilities form the entries of the confusion matrix. We discuss the impact of random noise on the CID process and present the results of applying the template/confusion matrix methodology to a few simple target representations. Specific attention is given to examining the relative issues associated with coherent and noncoherent target identification. For both coherent and noncoherent cases, approximate methods are developed to permit efficient computation of the confusion matrix entries, and the conditions for which these approximations are valid are discussed. Finally, we discuss several real-world, practical issues associated with the template-based methodology and the CID process.						
15. SUBJECT TERMS Coherent and noncoherent processing, combat identification, confusion matrices, Fisher Linear Discriminant, matched filter						
16. SECURITY CLASSIFICATION OF:			17. LIMITATION OF ABSTRACT	18. NUMBER OF PAGES	19a. NAME OF RESPONSIBLE PERSON J. Kent Haspert	
a. REPORT Uncl.	b. ABSTRACT Uncl.	c. THIS PAGE Uncl.	U/L	64	19b. TELEPHONE NUMBER *(include area code)* 703-845-2427	

Standard Form 298 (Rev. 8-98)
Prescribed by ANSI Std. Z39.18